USAAVSCOM TR-88-D-2

US ARMY
AVIATION
SYSTEMS COMMAND

ANALYTICAL AND EXPERIMENTAL INVESTIGATION OF RINGLESS PISTON CONCEPT

Daniel W. Dickey, Charles D. Wood
SOUTHWEST RESEARCH INSTITUTE
6220 Culebra Road
San Antonio, TX 78284

March 1988

Final Report for Period September 1986 - November 1987

Prepared for

AVIATION APPLIED TECHNOLOGY DIRECTORATE
US ARMY AVIATION RESEARCH AND TECHNOLOGY ACTIVITY (AVSCOM)
Fort Eustis, VA. 23604-5577

AVIATION APPLIED TECHNOLOGY DIRECTORATE POSITION STATEMENT

This report provides documentation for and evaluation of the ringless piston engine concept. This effort has demonstrated the feasibility of ringless piston operation in a two-stroke reciprocating engine and methods of improved performance. The results of this program will be used to support the Compound Cycle Turbo-Diesel Engine (CCTDE) program.

Mr. T. Dru Stowe of the Propulsion Technical Area, Aeronautical Technology Division, served as project engineer for this effort.

UNCLASSIFIED

SECURITY CLASSIFICATION OF THIS PAGE

REPORT DOCUMENTATION PAGE

Form Approved
OMB No. 0704-0188
Exp. Date: Jun 30, 1986

1a. REPORT SECURITY CLASSIFICATION Unclassified	1b. RESTRICTIVE MARKINGS None
2a. SECURITY CLASSIFICATION AUTHORITY N/A	3. DISTRIBUTION/AVAILABILITY OF REPORT Approved for public release; distribution is unlimited.
2b. DECLASSIFICATION/DOWNGRADING SCHEDULE N/A	
4. PERFORMING ORGANIZATION REPORT NUMBER(S) Report No. SwRI-1362	5. MONITORING ORGANIZATION REPORT NUMBER(S) USAAVSCOM TR 88-D-2
6a. NAME OF PERFORMING ORGANIZATION Southwest Research Institute 6b. OFFICE SYMBOL (If applicable) Div. 03	7a. NAME OF MONITORING ORGANIZATION Aviation Applied Technology Directorate U.S. Army Avn Res & Tech Acty (AVSCOM)
6c. ADDRESS (City, State, and ZIP Code) 6220 Culebra Road San Antonio, TX 78284	7b. ADDRESS (City, State, and ZIP Code) Fort Eustis, VA 23604-5577
8a. NAME OF FUNDING/SPONSORING ORGANIZATION U.S. Army Aviation Research and Technology Activity 8b. OFFICE SYMBOL (If applicable) SAVRT-R	9. PROCUREMENT INSTRUMENT IDENTIFICATION NUMBER DAAJ02-86-C-0030 DAAK70-85-C-0007
8c. ADDRESS (City, State, and ZIP Code) Ames Research Center Moffett Field, CA 94035	10. SOURCE OF FUNDING NUMBERS PROGRAM ELEMENT NO. 62209A; PROJECT NO. 1L162209AH76; TASK NO. C; WORK UNIT ACCESSION NO. 044EK

11. TITLE (Include Security Classification)

Analytical and Experimental Investigation of Ringless Piston Concept (U)

12. PERSONAL AUTHOR(S)

Dickey, Daniel W. and Wood, Charles D.

13a. TYPE OF REPORT	13b. TIME COVERED	14. DATE OF REPORT (Year, Month, Day)	15. PAGE COUNT
Final	FROM 9/26/86 TO 11/29/87	March 1988	48

16. SUPPLEMENTARY NOTATION

This report was also published as Interim Report BFLRF No. 247, sponsored by Belvoir Research, Development and Engineering Center, Fort Belvoir, VA.

17. COSATI CODES		
FIELD	GROUP	SUB-GROUP

18. SUBJECT TERMS (Continue on reverse if necessary and identify by block number)

Engine, Compound Engine, Piston, Reciprocating Engine, Piston Ring, Ringless Piston

19. ABSTRACT (Continue on reverse if necessary and identify by block number)

The purpose of this project was to analytically and experimentally investigate the concept of a ringless piston internal combustion engine. A joint objective was to design, build, and test a ringless piston to improve ringless piston engine performance. A computer model was developed to predict ringed and ringless piston engine performance. Experimental performance data were then collected by operating a small, liquid-cooled, two-stroke gasoline engine with and without the piston ring on the stock aluminum and Southwest Research Institute prototype steel piston. The experimental performance data were then compared with the results of the computer model. The results showed that a piston engine can operate without piston rings. Ringless piston engine power and efficiency were found to be defined by the expression C/NBS, where C = piston-to-bore diametrical clearance, N = engine speed in rpm, B = engine bore, and S = engine stroke. There was good agreement between predicted and measured performance results. The results of the prototype steel piston tests showed that ringless piston engine performance can be improved by using piston and liner materials that have similar coefficients of thermal expansion.

20. DISTRIBUTION/AVAILABILITY OF ABSTRACT	21. ABSTRACT SECURITY CLASSIFICATION	
☐ UNCLASSIFIED/UNLIMITED ☒ SAME AS RPT. ☐ DTIC USERS	Unclassified	
22a. NAME OF RESPONSIBLE INDIVIDUAL T. Dru Stowe	22b. TELEPHONE (Include Area Code) (804) 878-3073	22c. OFFICE SYMBOL SAVRT-TY-ATP

DD FORM 1473, 84 MAR

83 APR edition may be used until exhausted.
All other editions are obsolete.

SECURITY CLASSIFICATION OF THIS PAGE

UNCLASSIFIED

FOREWORD

The work reported herein was conducted at Southwest Research Institute for the Belvoir Fuels and Lubricants Research Facility (BFLRF) at Southwest Research Institute (SwRI), San Antonio, TX. The work was funded by the U.S. Army Aviation Research and Technology Activity under Contract No. DAAJ02-86-C-0030 and by the U.S. Army Belvoir Research, Development and Engineering Center (Belvoir RDE Center) under Contract No. DAAK70-85-C-0007. Mr. T. Dru Stowe of the Aviation Applied Technology Directorate served as technical monitor for the first contract, and Mr. M.E. LePera, Chief, Fuels and Lubricants Division, Belvoir RDE Center, STRBE-VF, served as technical monitor for the second contract. Mr. F.W. Schaekel, STRBE-VF, served as Contracting Officer's Representative.

ACKNOWLEDGMENTS

The authors would like to thank Dr. Bill Andre for his support and to acknowledge A. Rittimann for his contribution of engine installation, S. Almaraz, J. Sealey, and P. Quipp for engine instrumentation and data acquisition, G. O'Neal for steel piston design, J. Handfield of the BEL-RAY Company, Inc. for supplying the two-stroke synthetic lubricant, Alamo Cycle Sales for their prompt service in supplying engine parts, and N. Broussard, S. Douvry, and L. Pierce for preparation of the final report.

TABLE OF CONTENTS

LIST OF ILLUSTRATIONS

LIST OF ILLUSTRATIONS (Cont'd)

LIST OF TABLES

I. INTRODUCTION

Operating an engine without rings would solve the problem of short ring life that occurs at high engine speeds and loads. Engine life would then be extended to the life of the next critical engine component.

This project was designed to examine the ringless piston concept by analytically and experimentally comparing ringless piston engine performance with ringed piston engine performance. A computer model was developed to simulate ringless piston engine operation. The model used a leaking cylinder to simulate blowby past a ringless piston. Experimental performance data were then collected by operating a small, liquid-cooled, two-stroke gasoline engine with and without the piston ring on the stock aluminum piston. A joint objective of this project was to design, build, and test a ringless piston to improve ringless piston engine performance and to increase the piston's high-temperature capability. The experimental performance data were then compared with the results of the computer model.

The results of this project will help to predict ringless piston engine performance as a function of engine speed, bore, stroke, compression ratio, and piston-to-bore clearance.

A. Background

Engine life is detrimentally affected by high brake mean effective pressure (BMEP) and high piston speeds. The main source for wear at these operating conditions occurs at the interface between the piston ring and liner. Wear occurs primarily during reversal of ring travel direction at top dead center where the oil film between the ring and liner becomes very thin and metal-to-metal contact occurs.

The U.S. Army Aviation Systems Command (AVSCOM) funded a study to investigate the possibility of using a compound cycle engine (CCE) for helicopter application. A schematic of the CCE is shown in Fig. 1. The diesel core specifications are given in TABLE 1. A description of the engine is as follows:

> "A Compound Cycle Engine (CCE) as shown in Fig. 1 combines the airflow capacity and light-weight features of a gas turbine with the highly efficient, but heavier, diesel. The compressor of the gas turbine module delivers high-pressure air to the diesel core where further compression takes place in the cylinders (as with a conventional reciprocating compressor). Fuel is introduced and burned at very high pressure and temperature, and power is extracted in the downstroke of the diesel piston. The discharge gas, with its remaining energy, then is ducted to turbines that drive the compressor and also augment the output of the diesel core. The term "compound cycle," therefore, is an expression used to describe the process in which excess power is extracted from the turbomachinery and compounded through gearing to add to the output of the diesel core."(1)

This study was conducted jointly with NASA and under contract with Garrett Turbine Engine Company (GTEC). In an Executive Summary (Contract No. NAS3-24346-21-9854),

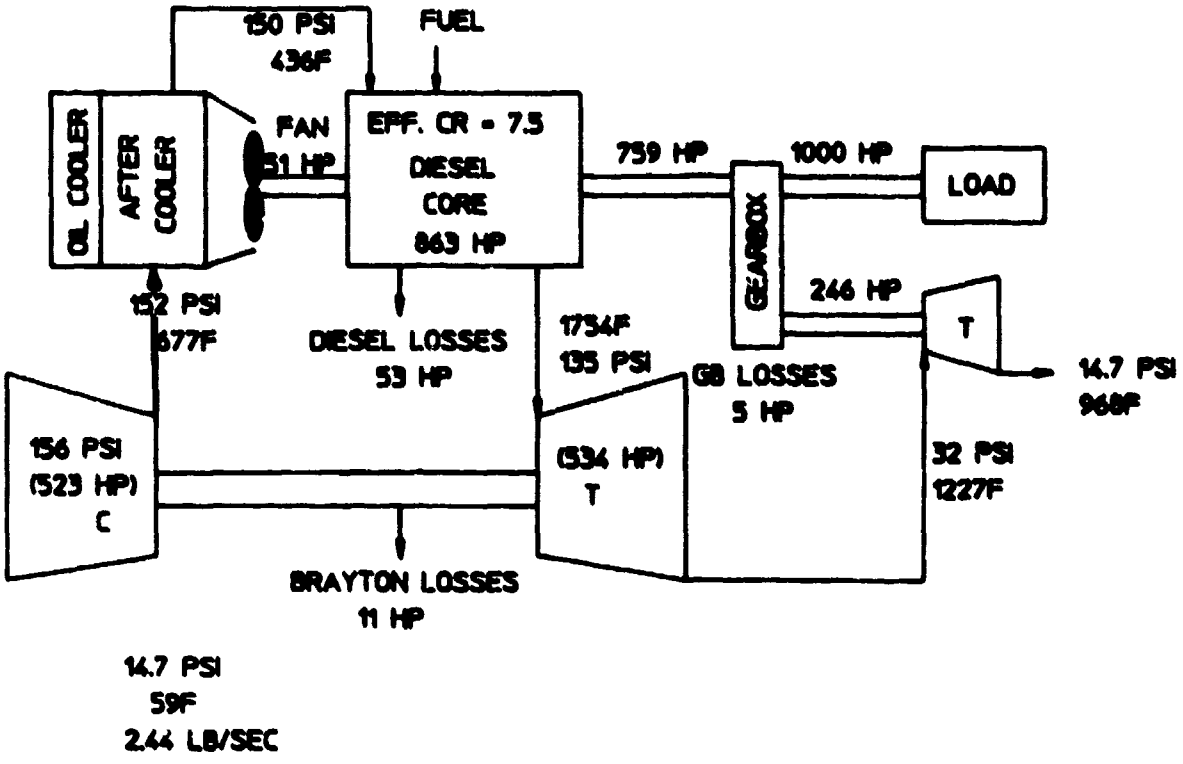

Figure 1. Compound cycle engine schematic.

TABLE 1. DIESEL CORE SPECIFICATIONS FOR COMPOUND CYCLE ENGINES

Output Horsepower	-	1000
Engine RPM	-	6122
Airflow Rate, lb/sec	-	2.44
Bore, in.	-	3.10
Stroke, in.	-	2.94
No. of Cylinders	-	6
Displacement, in^3	-	133.2
Equivalence Ratio	-	0.68
Peak Firing Pressure, P_{max}, psia	-	3362
Effective Compression Ratio	-	7.5
BMEP, psi	-	393

GTEC stated that ". . . the number one development challenge or life-limiting factor of most concern is the wear rate of the piston ring/liner interface materials."(1) In order to reduce the ring/liner wear, Southwest Research Institute (SwRI) proposed to investigate the concept of a ringless piston engine. Without rings, the unit contact pressure between the piston and bore, and similarly the wear rate, would be greatly reduced. Removing the piston rings, therefore, has the potential of increasing engine

life. SwRI proposed to eliminate the piston rings because both experience and theory indicate that piston rings may not be required at high engine speeds. At high speeds, the time for one cycle is so short that only a small percentage of the cylinder gases leak past the piston (blowby) during the cycle. Another potential advantage of removing the piston rings is to reduce the engine's mechanical friction. It is well known that the piston rings in conventional engines contribute 20 to 45 percent of the total mechanical friction.(2) If the losses due to ring friction could be eliminated, the engine has the potential for increased maximum power and efficiency.

While removing the piston rings has the potential of increasing engine life, reducing engine mechanical friction, and increasing engine power and efficiency, there are some potential problems. The hot running clearance between the piston and liner must be controlled and maintained at a smaller clearance than used by conventional engines to minimize blowby. Without piston rings, leakage at low engine speeds may be high and starting at conventional cranking speeds may be difficult. However, the compound cycle engine has the capability to be heated and cranked at high speeds using the compounded turbine. This technique should provide acceptable starting for the CCE.

Therefore, the potential benefits from a successful ringless engine are:

- Increased engine life through a reduction in ring/liner wear
- Increased power output and efficiency due to reduced friction.

The potential problems are:

- Control of hot running clearance between the piston and liner
- High blowby at low engine speeds
- Cold starting at conventional cranking speeds.

B. Objective

The purpose of this project was to analytically and experimentally investigate the concept of a ringless piston internal combustion engine. A joint objective was to design, build, and test a ringless piston to improve ringless piston engine performance.

II. COMPUTER SIMULATION OF A RINGLESS PISTON ENGINE

A computer program was written to analytically predict the performance of an engine running with and without piston rings. The computer model simulated blowby using a perfectly sealed piston in a leaking cylinder with a leak hole area A. The leak hole area for a ringless piston was determined using the diametrical piston-to-bore clearance and the cylinder bore diameter. The leak hole area for a ringed piston was assumed to be zero. Some other assumptions for the SwRI-developed computer model were:

- The working fluid was air with constant specific heats.
- Ringed and ringless engine frictions were equal and constant.
- The intake and exhaust processes were not accounted for.
- The model used a constant overall heat transfer coefficient to simulate heat losses to the surroundings.
- The mass of fuel injected and subsequent dissociation during combustion were ignored.
- The heat release rate was simulated using an isosceles triangular heat release shape.

The input parameters for the computer program included engine inlet temperature and pressure, speed, bore, piston-to-bore clearance, stroke, connecting rod length, compression ratio, fuel/air ratio, beginning of heat release angle, shape of heat release, and heat release duration. The program used these input parameters to determine the thermodynamic properties of the working fluid at bottom dead center (beginning of the compression stroke). The program then proceeded to calculate the thermodynamic state of the working fluid in a quasi-static manner for each degree of crankshaft rotation during one complete cycle of a two-stroke engine. The heat release period was simulated using an isosceles triangular heat release shape beginning 20 degrees before top dead center (BTDC) with a duration of 40 degrees crank angle. The appropriate flow equation for the leaking cylinder gas was determined by the program, depending on whether the flow was subsonic, sonic, or supersonic.

One result of the engine model is shown in Fig. 2, which is a plot of cylinder gas pressure versus crank angle for one complete cycle of a Suzuki two-stroke engine at 3000 rpm. The top curve shows the cylinder pressure for the ringed engine with a leak area equal to zero (or zero piston-to-bore clearance). The bottom curve shows the cylinder gas pressure for the ringless piston with a piston-to-bore diametrical clearance of 0.003 inch. The curves in Fig. 2 show that blowby (the amount of mass leaked) increases with increasing cylinder pressure.

An Indicated Mean Effective Pressure (IMEP) was calculated for each curve in Fig. 2. The IMEPs for the ringed and ringless piston curves were 124 and 54 psi, respectively. This change in IMEP corresponds to a power loss of 56 percent due to blowby that occurs in the ringless piston engine. It would be expected that the power loss due to blowby is closely related to the weight percent of cylinder gas leaked per cycle. For the ringless

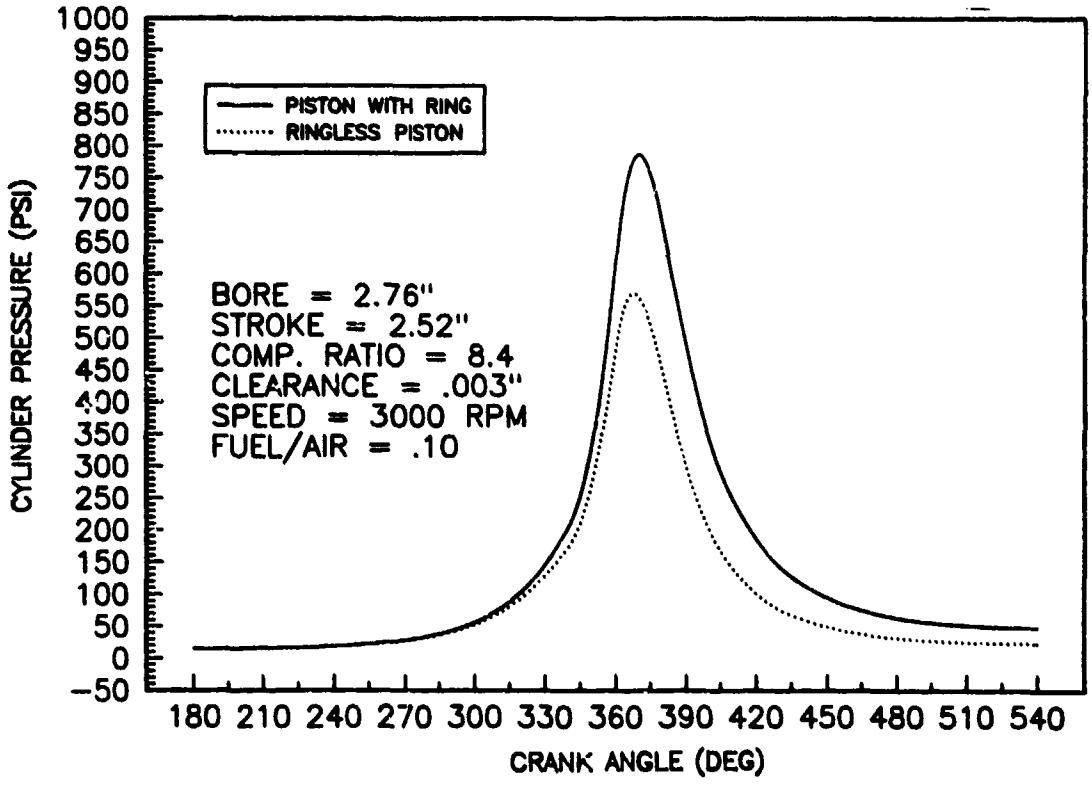

Figure 2. **Computer simulation of cylinder pressure versus crank angle for ringed and ringless pistons.**

piston, the weight flow rate of gas that leaks past the piston (W) is proportional to the flow area (A). The equation for the leak flow area is given by

$$A = \pi (B^2 - (B - C)^2)/4 \tag{1}$$

where B is the cylinder bore diameter and C is the diametrical piston-to-bore clearance. The weight of gas leaked per two-stroke engine cycle is W/N, where N is the engine speed in revolutions per minute. The weight of gas initially trapped in the cylinder (WI) is proportional to the cylinder displacement volume (V). The displacement volume is given by

$$V = \pi B^2 S/4 \tag{2}$$

where S is the engine stroke. The weight percent of gas leaked per cycle is then proportional to

$$\frac{W}{N(WI)} \tag{3}$$

Combining expressions (1), (2), and (3), it is found that the weight percent of gas leaked per cycle is also proportional to

$$\frac{C}{NBS} \tag{4}$$

Expression (4) defines the engine power loss due to gas leakage.

Expression (4) is plotted versus engine power ratio in Fig. 3. The power ratio is defined as the ringless piston (leaking cylinder) engine power divided by the ringed piston engine power. The curves in Fig. 3 are a result of the computer simulation for a range of engine bore diameters, strokes, speeds, compression ratios, and piston-to-bore clearance dimensions. Fig. 3 shows that the expression C/(NBS) does control the power loss due to blowby. Increasing the piston-to-bore clearance (C) increases the leak area and reduces the power ratio. Increasing the engine speed (N) reduces the time available per cycle for the gases to leak past the piston, which increases the power ratio. Increasing the engine bore and stroke also increases the power ratio by providing a larger initial cylinder gas volume. In general, the power ratio is approximately proportional to the bore diameter squared because the term BS in the denominator of expression (4) can be replaced with b^2 for most engines (i.e., the bore/stroke ratio of most engines is approximately 1.0). The effect of engine compression ratio on the power ratio is also shown in Fig. 3. Blowby increases with increasing compression ratio, and the increase in blowby reduces the power ratio.

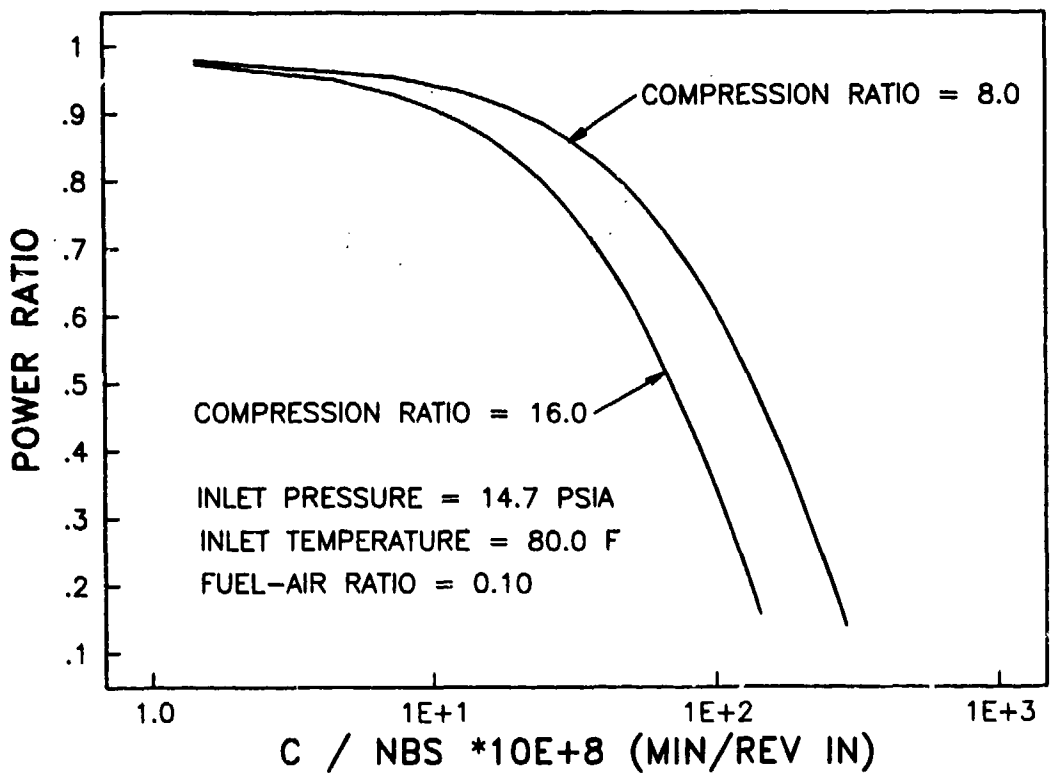

Figure 3. Computer simulation of engine power ratio versus C/NBS.

This analysis verifies that larger engines can tolerate larger piston-to-bore clearances than smaller engines. The allowable leak clearance is approximately proportional to the square of the engine bore diameter and is proportional to engine speed. The reduced leak sensitivity of high-speed engines is frequently observed in racing engines. Racing engines experience very little power loss at high speeds due to sealing problems such as

worn cylinder liners, burned valves, or stuck piston rings. Another example of reduced leak sensitivity in high-speed engines is observed with model airplane engines that operate without piston rings. Conversely, low-speed engines such as ship diesel engines have large bores and many piston rings to decrease their leak sensitivity.

Results from a computer simulation of engine power ratio versus engine speed for specific clearances are shown in Fig. 4. The curves show the effect of piston-to-bore clearance and engine speed on engine power ratio. The engine modeled in Fig. 4 is a Suzuki RM 250 cc two-stroke motorcycle racing engine with a bore of 2.76 inches (70.1 mm), a stroke of 2.52 inches (64.0 mm), and a geometric compression ratio of 8.4. The three curves in Fig. 4 represent piston-to-bore diametrical clearances of 0.001 (0.025), 0.002 (0.051), and 0.003 (0.076) inch (mm). Curves in Fig. 4 show that increasing the engine speed has a greater effect on increasing the engine power ratio at larger piston-to-bore clearances as evidenced by the slopes of the three curves. Also, for a given piston-to-bore clearance, the improvement in power ratio decreases with increasing engine speed.

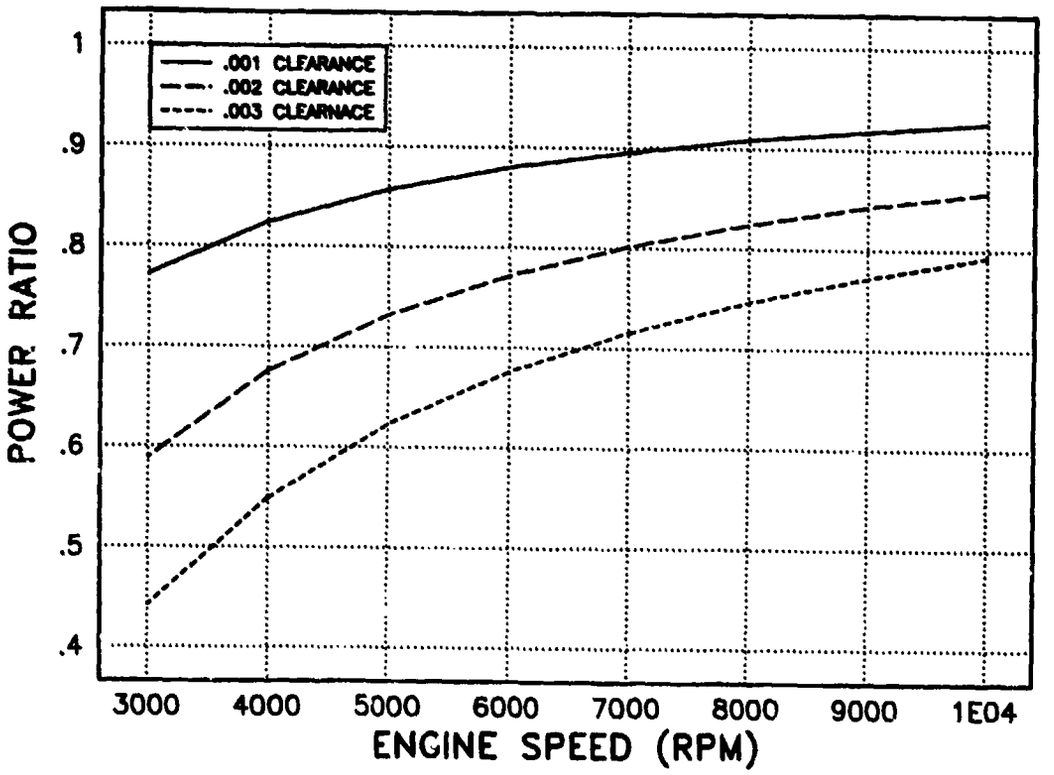

Figure 4. **Computer simulation of engine power ratio versus engine speed for the Suzuki engine at piston-to-bore diametrical clearances of 0.001, 0.002, and 0.003 inch.**

The SwRI-developed engine model provides a means of predicting the performance of a ringless engine as a function of engine speed, load, bore, stroke, compression ratio, and piston-to-bore clearance. The piston-to-bore clearance of an operating engine, however, may be very difficult to determine. As a first step in solving this problem, the hot running clearance can be predicted from a knowledge of the measured cold clearance and

the thermal expansion coefficients of the piston and liner materials. Fig. 5 is a plot of piston-to-bore diametrical clearance versus piston-liner interface temperature for the Suzuki engine that uses an aluminum piston and cast-iron liner. In Fig. 5, it was assumed that the piston and liner were at the same equilibrium temperature. In reality, a temperature gradient exists between the piston and liner and also from top to bottom of each component. A maximum piston-liner interface temperature of 350°F (177°C) was used in this plot due to the pronounced reduction in mechanical properties of the aluminum piston that occurs above this temperature.

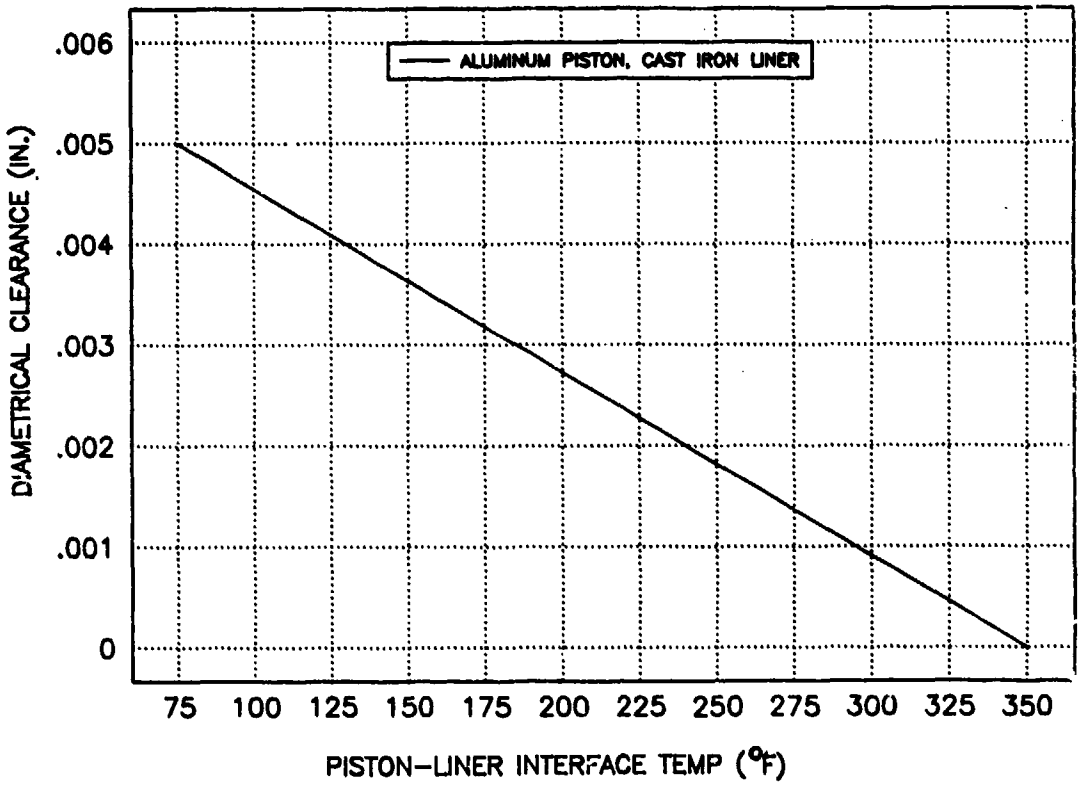

Figure 5. Diametrical piston-to-bore clearance versus piston-liner interface temperature for the engine using an aluminum piston and cast-iron liner.

A change in clearance due to temperature will affect ringless engine performance as shown in Fig. 4. As the piston temperature increases, the clearance will be reduced and the power output will increase. Conversely, ringless engine power will be reduced at reduced piston temperatures. The piston-to-bore clearance, then, is much more critical in a ringless engine, since this clearance controls engine power and efficiency. A successful ringless engine should provide some method of maintaining a constant minimum piston-to-bore clearance. The engine could be designed to operate at constant speed and load (i.e., constant piston temperature) or a superior solution would be to use piston liner materials with similar coefficients of thermal expansion. This configuration would allow the ringless engine to operate over a broad speed and load range without severely affecting the piston-to-bore clearance.

III. EXPERIMENTAL INVESTIGATION OF A RINGLESS PISTON ENGINE

An experimental investigation was conducted to collect ringed and ringless piston engine performance data. The experimental data were then compared with the results of the computer model used to simulate ringed and ringless piston operation.

The first step in the experimental investigation was to choose a suitable test engine that conformed to the contract requirements.

A. Test Engine Selection

The contract specified that the test engine must be single-cylinder, two-stroke, gasoline-powered, and water-cooled. Based on these requirements, a Suzuki RM 250 cc motorcycle engine was selected as the project test engine. The engine specifications are given in Table 2.

TABLE 2. SUZUKI RM 250-CC ENGINE SPECIFICATIONS

Engine Type:	Single-cylinder, two-stroke, liquid-cooled, full reed valve induction
Displacement:	246 cc
Bore and Stroke:	70 mm x 64 mm
Compression Ratio:	8.4:1
Number of Piston Rings:	1
Carburetor:	Mikuni VM38SS, flat slide
Lubrication:	Fuel/oil mixture
Ignition:	Suzuki Pointless Electronic Ignition ("PEI")
Starter:	Primary kick
Transmission:	5-speed gearbox

The motorcycle engine was selected because it is a very durable racing engine capable of 8000+ rpm operation. This engine uses a cast-iron cylinder liner that can be easily machined (see Fig. 6). Other similar racing engines produced by Honda, Kawasaki, Yamaha, Husqvarna, Can Am, and KTM were considered but not chosen because they all use some form of hard chrome-plated cylinder liner (such as Kawasaki's electrofused liner) that cannot be easily machined. The test engine was chosen because it is easier to bore and hone a cylinder liner than it is to OD-grind a piston when optimizing the piston-to-bore clearance. Two oversize pistons are also available from Suzuki for this engine. Top end replacement parts such as the cylinder, cylinder head, piston, and piston ring are

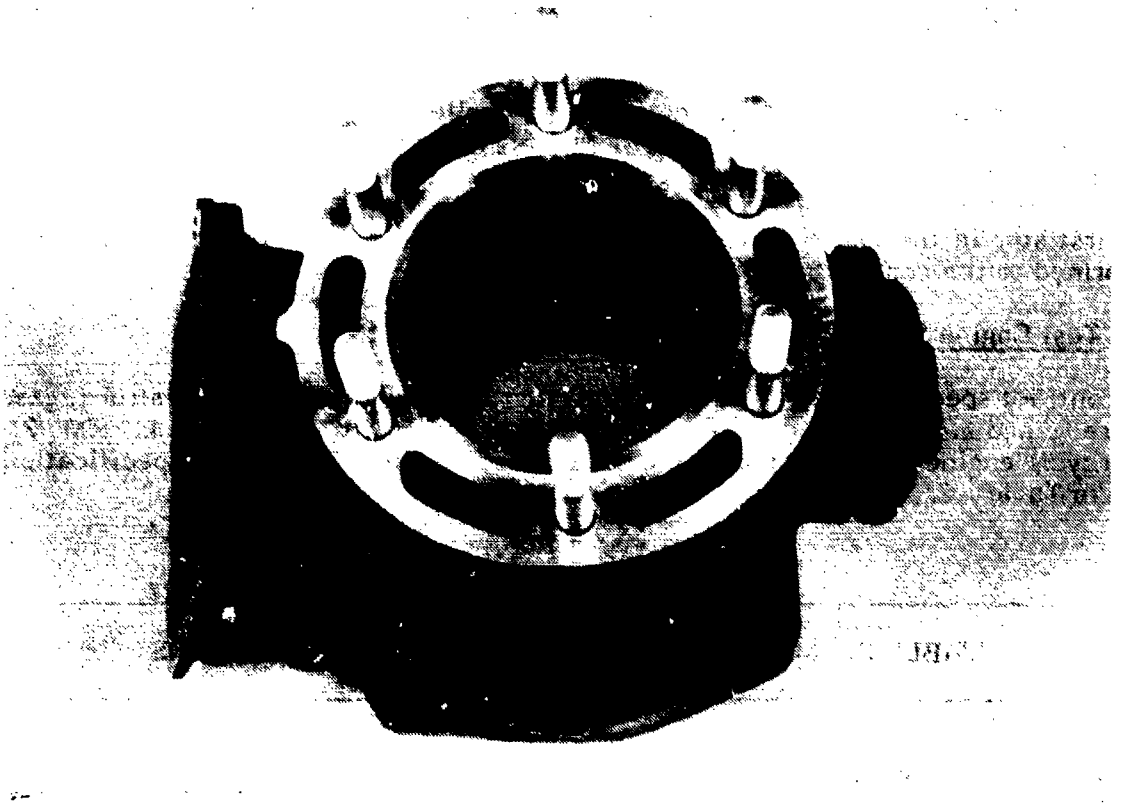

Figure 6. Photograph of Suzuki RM 250 cc engine cylinder liner.

readily available. The piston ring for this engine is a regular maintenance item. The factory suggests that the ring be replaced after every two races. Another reason for choosing a motorcycle engine is that the engine incorporates a five-speed manual transmission. The transmission increases starting speed capability and ensures a more reliable engine installation by reducing dynamometer and driveshaft speeds. Crankshaft-to-transmission output shaft gear reduction was 2.5:1 with the transmission in the highest (fifth) gear position.

B. Engine Setup

The motorcycle engine was installed in a test cell at SwRI as shown in Figs. 7 and 8. The engine's transmission output shaft was connected to the driveshaft by a sprag clutch and flexible coupling. The flexible coupling corrected for misalignment between the driveshaft and engine and also reduced torsional vibration. The sprag is a one-way clutch that allows the engine to turn the dynamometer but prevents the dynamometer's inertia from turning the engine. The sprag was an important safety factor because it prevented the dynamometer and driveshaft inertia from destroying the engine in the event of engine seizure. The other end of the driveshaft was connected to an eddy-current absorption dynamometer via another flexible coupling. An electric motor was connected to the engine output shaft using a drive belt, pulleys, and tensioner. The electric motor provided the cranking speeds required to start the engine in the ringless piston configuration. The tensioner was used to disengage the belt during engine tests. The engine cranking speed could be varied by changing the electric motor drive belt pulley and/or the engine transmission gear. The motorcycle engine also had a wet multi-plate clutch that allows the transmission gear to be changed during engine operation.

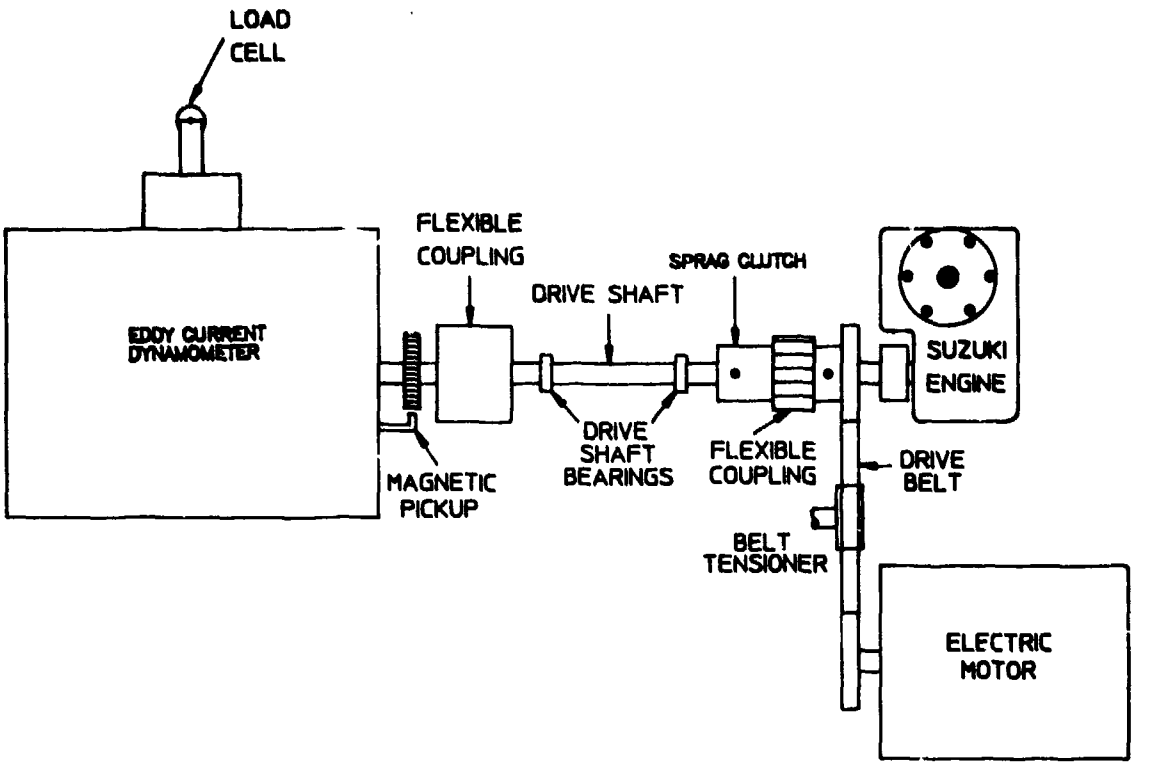

Figure 7. Schematic of the test engine installed in test cell No. 4.

Figure 8. Photograph of the motorcycle engine installed in test cell No. 4.

Fig. 9 is a schematic of the engine cooling and heating systems. A shell-tube heat exchanger was installed to replace the motorcycle engine's radiator. The shell-tube heat exchanger used a regulated supply of shop water to maintain a constant engine coolant temperature during engine operation. A separate water pump and electric water heater were also installed to preheat the cylinder liner and help maintain constant coolant temperature. Preheating the cylinder liner helped to prevent cold engine seizure during engine startup and enabled the engine to start easier in the ringless piston configuration.

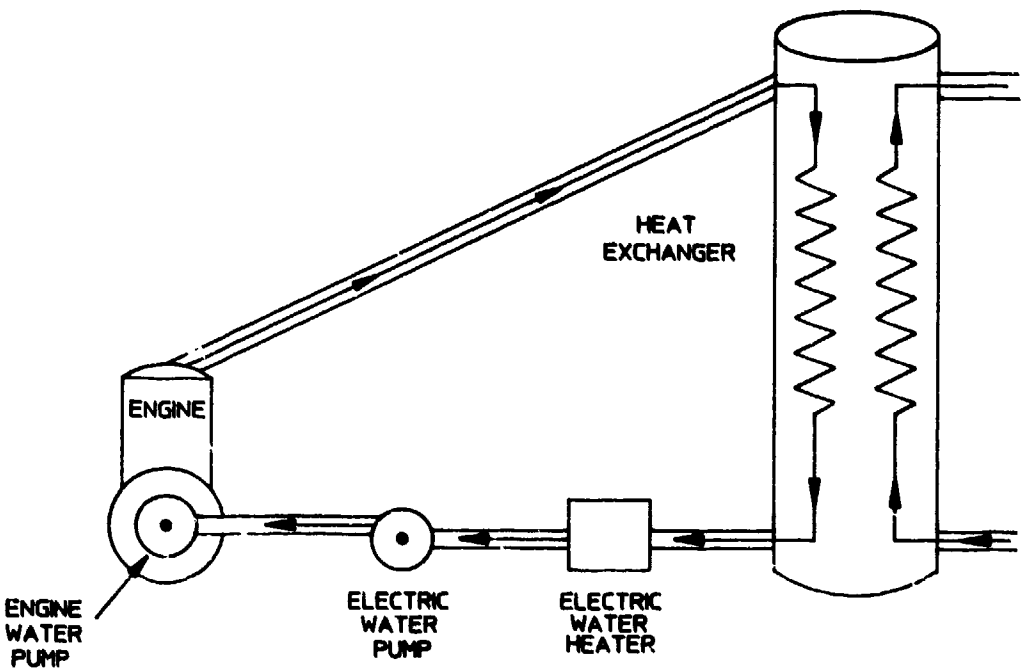

Figure 9. Schematic of the engine cooling and heating systems.

C. Engine Instrumentation

A schematic of the engine instrumentation is shown in Fig. 10. Engine intake airflow was measured using a precision gas flow nozzle. Initially, a Meriam laminar flow element was used, but it caused an excessive intake air restriction that severely limited the two-stroke engine's maximum power and adversely affected the part-load performance. The precision gas flow nozzle eliminated these problems by operating at a much lower pressure drop. The pressure drop across the nozzle was measured using an inclined manometer. Volumetric fuel flow was measured using a burette and stopwatch. Engine speed was measured using a magnetic pickup and 60-tooth gear mounted on the driveshaft. A strain gage-type load cell was used to measure engine load.

A Kistler Model 6121 pressure transducer was mounted in the cylinder head to measure cylinder pressure. Engine crank angle position was measured by mounting a magnetic pickup next to the engine flywheel. The engine flywheel was removed and modified to accept an aluminum disk with 12 steel inserts. Two magnetic pickups were then mounted near this disk to detect the steel inserts. One magnetic pickup was used to produce eleven voltage pulses at 10-degree crank angle increments for display on the oscillo-

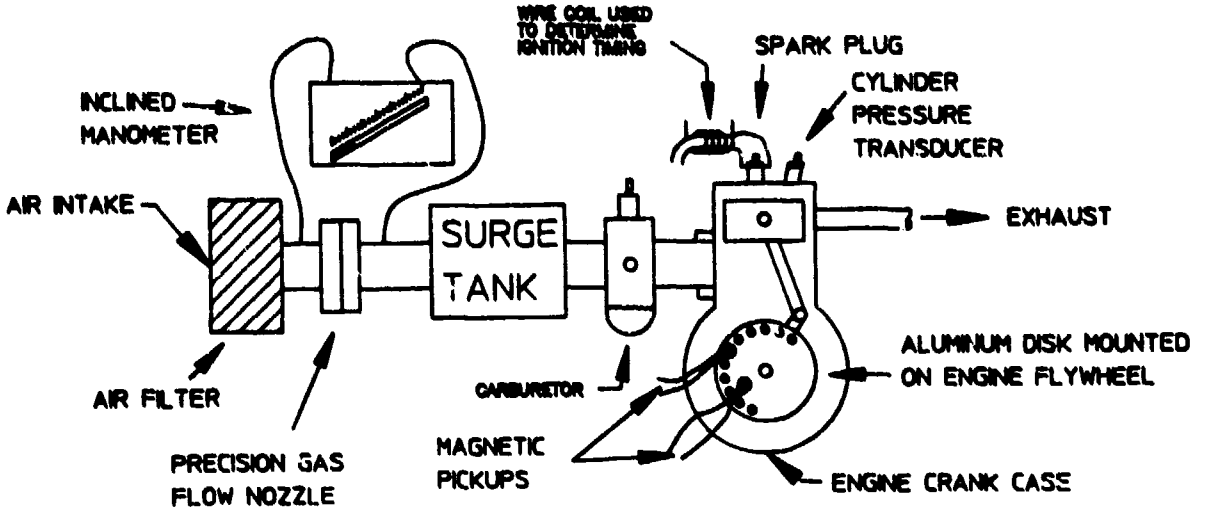

Figure 10. Schematic of the engine instrumentation.

scope. The second magnetic pickup was used to trigger the oscilloscope, which displayed the cylinder pressure, crank angle, and ignition timing traces. The ignition timing trace was produced by wrapping a wire around the high tension spark plug wire and connecting it to a channel of the oscilloscope.

Engine intake air, exhaust, coolant inlet and coolant outlet temperatures were measured using K-type thermocouples and an Omega temperature recorder.

D. Engine Test Procedure

The engine test was conducted as follows. First, the stock engine was disassembled. The piston-to-bore clearance was measured with a micrometer perpendicular to the piston pin at a point halfway down the piston and liner. The engine was then assembled using the stock aluminum piston and ring. Before starting the engine, the dynamometer load cell was calibrated by setting the zero and adjusting the span using a deadweight. The inclined manometer used to measure intake airflow was also zeroed. The external water pump and heater were then turned on to preheat the engine coolant. The coolant water was preheated to reduce engine warmup time and to prevent cold engine seizure. The engine was started by first turning on the electric starting motor. The motorcycle engine clutch was then disengaged with the transmission in the highest (fifth) gear position. This gear resulted in a primary reduction of 2.565 between the engine crankshaft and dynamometer driveshaft. The belt tensioner was used until the driveshaft reached maximum speed of approximately 3000 rpm. The motorcycle clutch was then

engaged to start the engine. The drive belt was disengaged and the electric motor turned off during the performance tests. The dynamometer controller was used in the speed control mode to set the desired test speed. The engine load was set using the engine throttle. The engine throttle position was controlled using a regulated air supply and an air cylinder connected to the Mikuni carburetor slide. The engine was allowed to stabilize for several minutes. During this time the water flow through the coolant heat exchanger was adjusted to maintain a constant cylinder head outlet temperature of 180°F (82°C).

Engine performance data were recorded at five engine speeds of 3000, 4000, 5000, 6000, and 7000 rpm and four engine loads (100, 75, 50, and 25 percent of maximum power at the given engine speed). The performance data recorded at each data point included engine speed, load, intake air temperature, exhaust gas temperature, inlet and outlet coolant temperatures, barometric pressure, and the pressure drop across the precision gas flow nozzle. A photograph was also taken of the oscilloscope, which simultaneously displayed the cylinder pressure and crank angle markers located at 10-degree intervals. Three fuel flow measurements were taken per data point by measuring the time required for the engine to consume a specified volume of fuel.

E. Engine Test Results

The engine was first tested using the stock aluminum piston and ring. The engine was assembled with a cold piston-to-bore diametrical clearance of 0.0045 inch (0.1143 mm). All of the data points were completed except, at the 7000 rpm, 25 percent load condition, where only the engine speed and load were recorded. Engine air and fuel flow measurements were not recorded because the engine seized before the data point could be completed. The engine seizure was probably the result of an excessively lean air/fuel ratio at the 25-percent load condition. Unfortunately, airflow and fuel flow measurements could not be recorded to substantiate this theory.

The cylinder head, liner, and piston were then removed, cleaned, and inspected. The cylinder liner was gently honed to remove scratches. The aluminum piston was slightly scuffed and replaced with a new one. The piston-to-bore clearance was then measured using the honed liner and new aluminum piston. The new piston-to-bore diametrical clearance was 0.0033 inch (0.084 mm). This clearance was smaller than the previous test clearance of 0.0045 inch (0.1143 mm) because a new piston was used. The recommended piston-to-bore clearance for the engine varies from 0.0024 inch (0.061 mm) to a wear limit of 0.0047 inch (0.119 mm).

The engine was then assembled without the piston ring and an attempt was made to start the engine using a cranking speed of approximately 3000 rpm. The engine was motored at this speed for approximately 10 seconds before the engine speed increased to the preset dynamometer control speed of 4000 rpm. The engine started and ran smoothly. The 10-second delay in engine starting was required for the combustion gases to heat up the aluminum piston and reduce the piston-to-bore clearance. Once the piston-to-bore clearance was reduced to some maximum value, the engine could run with an acceptable amount of blowby.

An attempt was then made to repeat the data points taken with the ringed piston. The full-load data points and most of the 75-percent-load data points could not be repeated due to the loss of engine power associated with blowby past the ringless piston. The same part-load data points were repeated so that ringed and ringless piston engine efficiency could be compared at the same power output. Only the engine speed and load

were recorded at the 7000 rpm, full load condition because the engine seized before a full data set could be recorded. The engine seizure could possibly be attributed to several factors. The ringless engine was assembled with a smaller piston-to-bore clearance (0.0033 inch) (0.0838 mm) versus the ring engine (0.0045 inch) (0.1143 mm). The smaller initial clearance could have caused the seizure at the full load condition. The seizure may also be attributed to the operating characteristics of the ringless piston. Without a piston ring there may be less heat transfer from the piston to the liner, which would result in higher piston temperatures and possible seizure. The piston temperature may also have increased due to heating from the blowby gas. The engine seizure may also be attributed to an excessively lean mixture for the ringless engine although the air-fuel ratio could not be recorded before the engine seized to substantiate this theory. The same carburetor jetting was retained for the ringless piston tests so comparisons in specific fuel consumption could be made between the ringed and ringless engine tests. In summary, it could not be concluded that the engine seizure was due to ringless operation. The engine seizure could probably have been prevented by using a larger initial piston-to-bore clearance.

1. Maximum Power Performance Results

The full power performance results for the stock aluminum piston are shown in Fig. 11. The aluminum piston test data are given in Tables A-1 and A-2 of Appendix A. Fig. 11 is a plot of corrected brake horsepower versus engine speed for the engine running at wide open throttle with and without the piston ring on the stock aluminum piston. As shown, the engine power ratio (previously defined as ringless engine power divided by ringed engine power) increased with engine speed as predicted. The power ratio increased from 0.56 at 3000 rpm to 0.89 at 7000 rpm. In other words, the engine produced 56 and 89 percent of the stock engine power running without the piston ring at 3000 and 7000 rpm, respectively. The effect of engine speed on power ratio is more clearly shown in Fig. 12, which is a plot of engine power ratio versus engine speed corresponding to Fig. 11. (Fig. 12 shows the effect of both engine speed and piston-to-bore clearance on the engine power ratio because the piston-to-bore clearance is reduced at high loads due to increased piston temperatures.) Fig. 12 shows that the power ratio increased with engine speed except at the 5000 rpm operating condition. The reduction in power ratio at 5000 rpm can be explained by the fact the engine did not perform well at 5000 rpm. The decrease in engine power ratio was attributed to an inexplainable reduction in combustion efficiency. Evidence for the poor combustion efficiency at 5000 rpm is shown in Fig. 13, which is a plot of exhaust gas temperature versus engine speed for the ringed and ringless piston engines. The data in Fig. 13 show that the exhaust gas temperature increased only slightly at 5000 rpm just as the engine power increased in Fig. 12. The decrease in combustion efficiency resulted in lower piston temperature and a greater piston-to-bore clearance. Thus, the power ratio decreased at 5000 rpm due to a reduction in combustion efficiency, which resulted in larger piston-to-bore clearance and increased blowby.

The most important result of the experimental data is that the two curves in Fig. 11 are converging. Evidence for this convergence is shown by the positive slope of the power ratio curve in Fig. 12. The convergence suggests that there may be an engine speed where the ringless piston engine power equals or exceeds the ringed engine power, which would correspond to a power ratio equal to or greater than 1.0. At a power ratio greater than or equal to 1.0, the power gain due to a reduction in piston ring-liner friction would become greater than or equal to the engine power losses due to blowby. Power ratios greater than 1.0 were not predicted by the computer model because the model does not account for changes in mechanical friction when the engine is run in the ringless

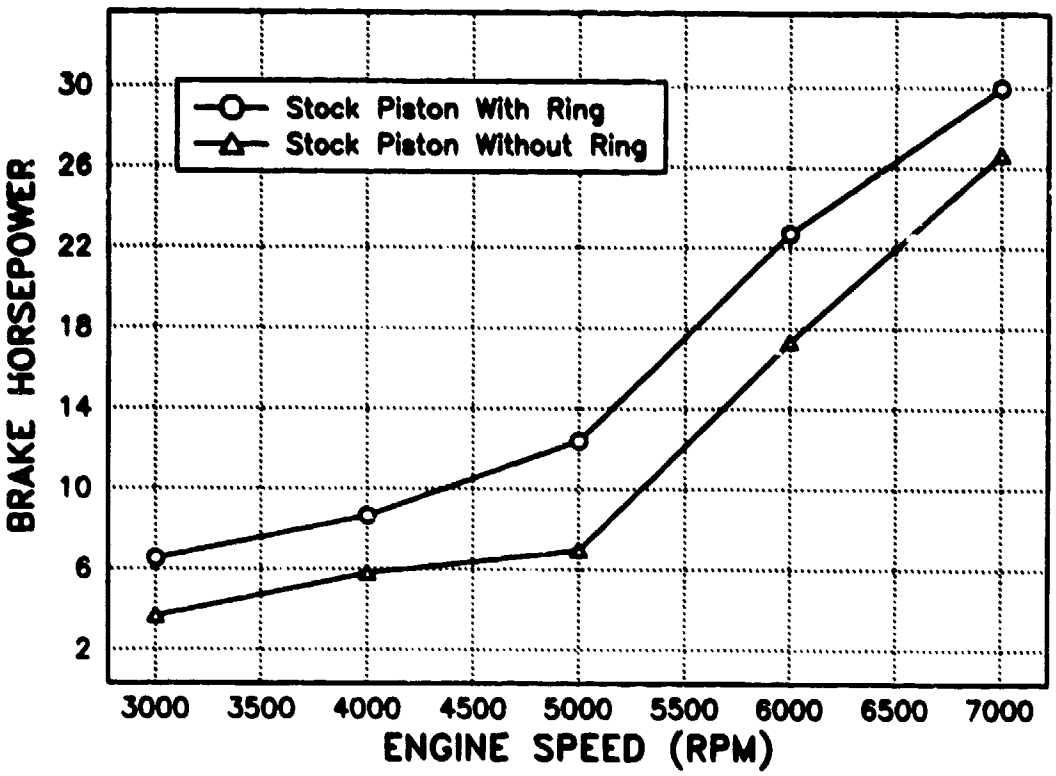

Figure 11. Full power curves for the test engine running with and without the piston ring.

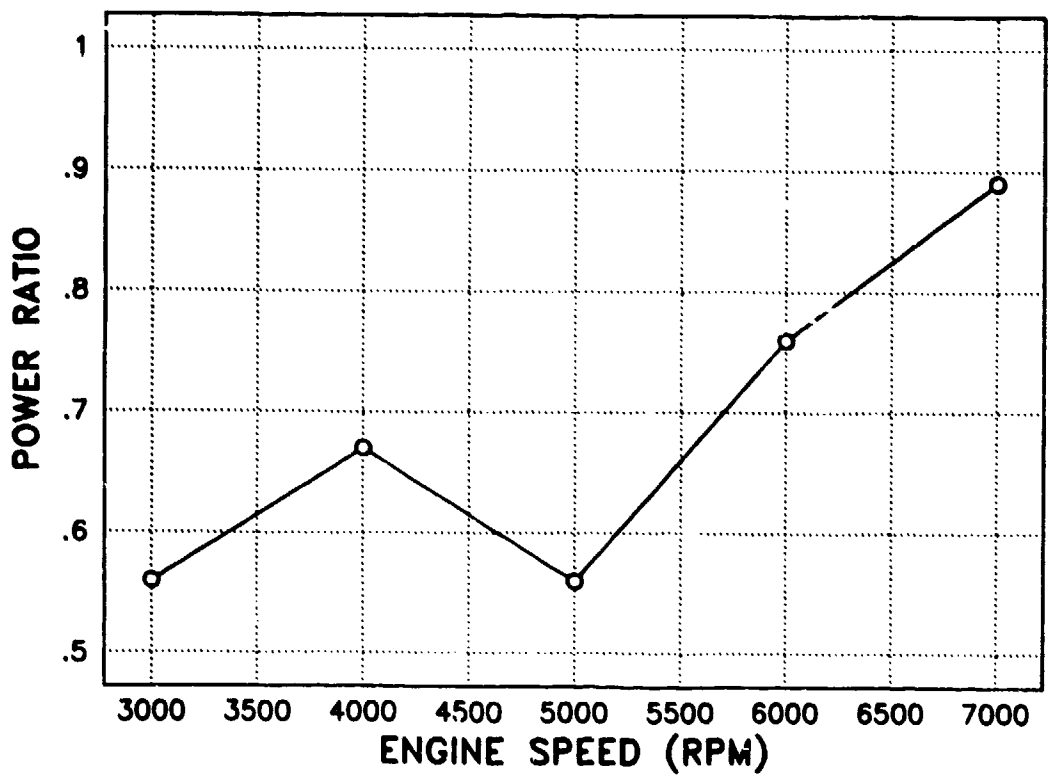

Figure 12. Power ratio versus engine speed for the test engine running at wide open throttle.

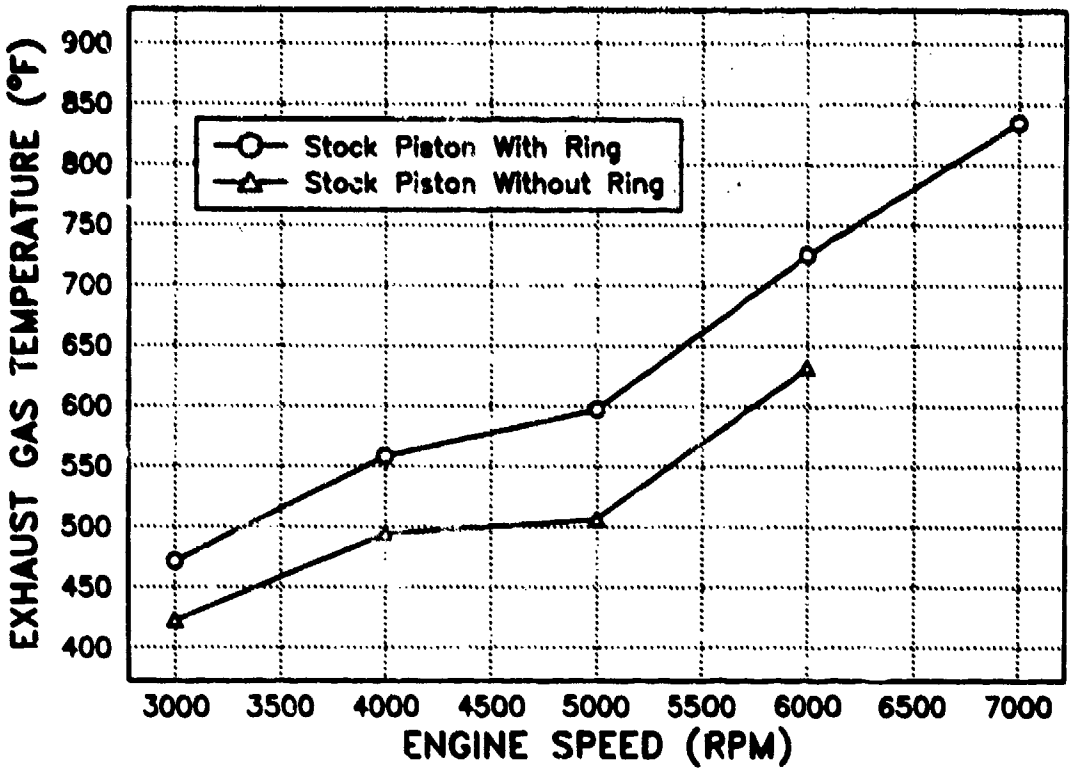

Figure 13. Exhaust gas temperature versus engine speed for the test engine running at wide open throttle.

configuration. The engine speed where the power ratio equals 1.0, however, can perhaps be extrapolated from the experimental engine data because the data do include the change in engine friction. As a rough estimate of the engine speed corresponding to a power ratio of 1.0, a linear curve fit was applied to the data points shown in Fig. 12. The equation for this curve was then solved for the engine speed corresponding to a power ratio of 1.0. The solution to the linear curve fit equation was an engine speed of 9055 rpm. A linear curve fit was again applied to the data points in Fig. 12 without the data point at 5000 rpm because this point did not follow the trend of increasing power ratio with engine speed. The engine speed corresponding to a power ratio of 1.0 in this case was 8649 rpm. It is difficult to determine whether or not a power ratio of 1.0 can actually be achieved at these engine speeds. At higher engine speeds, the engine produces more power, which reduces the piston-to-bore clearance. By extrapolating the power ratio curve, it was assumed that the same initial piston-to-bore clearance can be used to obtain the increased engine speeds. However, using the same initial clearances may cause the engine to seize before reaching engine speeds of 8649 and 9055 rpm. The actual crossover speed (speed where the ringless and ringed piston engine power curves intersect, i.e., power ratio equals 1.0) for this engine will probably be greater than these estimates of 8649 and 9055 rpm, since it will be necessary to start with a larger initial piston-to-bore clearance.

The crossover speed for the test engine is high because it has a small bore and, more importantly, uses only one piston ring to minimize friction between the ring and liner.

The crossover speed for larger bore engines that use multiple piston rings should be considerably lower for two reasons:

(1) As was shown earlier in this report, the power ratio increases approximately as a function of the bore squared. Therefore, a large bore engine has reduced leak sensitivity, which will improve the power ratio at lower engine speeds.

(2) Engines that use several piston rings have a larger percentage of their total mechanical friction due to ring-liner friction compared to the test engine that uses only one piston ring.

2. Efficiency

The efficiency of the engine running with and without the piston ring was compared using the brake specific fuel consumption (BSFC). The BSFC includes the change in engine friction when the piston ring was removed. A complete list of the aluminum piston BSFC data is given in Appendix A.

Fig. 14 is a plot of BSFC versus brake mean effective pressure (BMEP) for the engine running with and without the piston ring at 6000 rpm. The data points for the two curves correspond to the same output power except at the full-load condition, where the ringless engine could not produce the same maximum power as the ringed engine. As

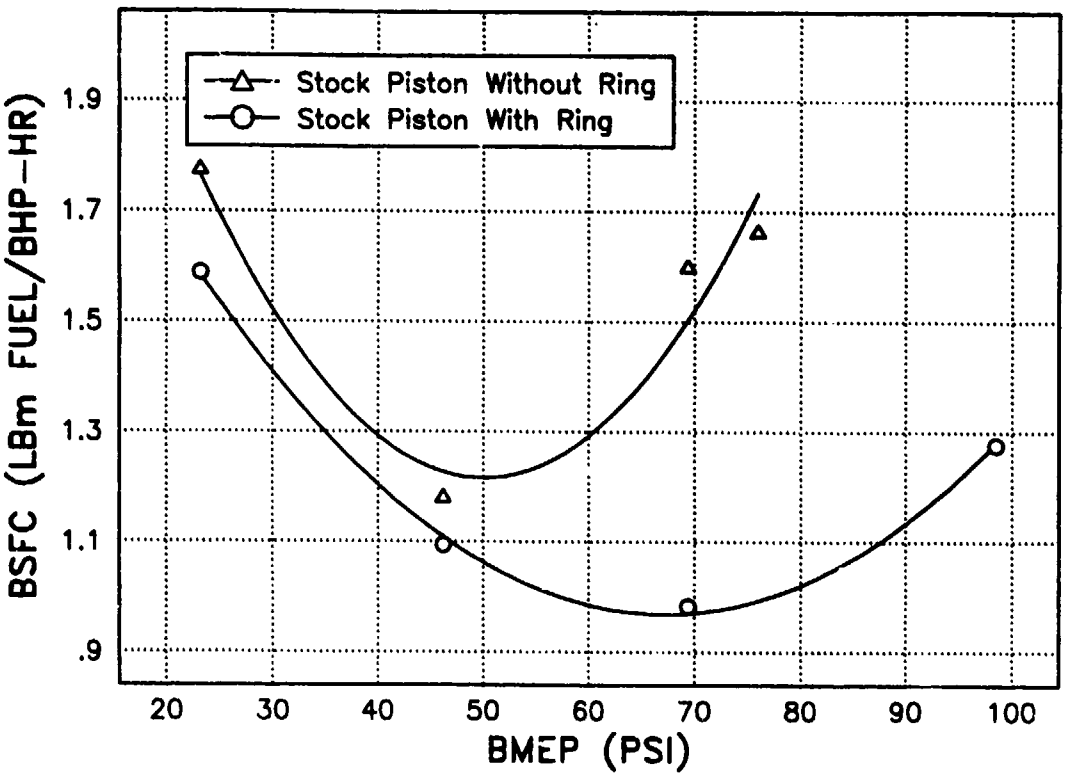

Figure 14. Brake specific fuel consumption versus brake mean effective pressure for the test engine running with and without the piston ring at 6000 rpm.

shown in Fig. 14, the BSFC increased when the engine was run without the ring. An increase in BSFC corresponds to a reduction in engine efficiency. The increase in BSFC for the ringless engine was greater at high loads due to the corresponding increase in blowby. At 6000 rpm, the ringless engine BSFC increased by 12 percent at the 25 percent load condition and by 63 percent at the 75 percent load condition compared to the ringed engine. The efficiency was reduced for the ringless engine because removing the ring increased the amount of blowby and reduced the cylinder gas pressure during the expansion stroke. Engine efficiency was also reduced during the compression stroke because an increase in blowby during compression lowered the engine's effective compression ratio. In order for the ringless piston engine to make up for this loss of engine efficiency and power due to blowby, the throttle had to be opened so the ringless engine could produce the same power as the ringed engine (except at the 100 percent load condition), as shown in Fig. 14. Increasing the throttle opening for the ringless engine increased the intake airflow and thus fuel flow for this homogeneously charged engine. The increase in airflow is shown in Fig. 15, which is a plot of intake airflow versus BMEP for the test engine at 6000 rpm running with and without the piston ring. As shown in Fig. 15, the intake airflow for the ringless engine increased by 34 percent at the 75 percent load condition (approximately 70 psi BMEP), which contributed to the 63 percent increase in BSFC shown in Fig. 13.

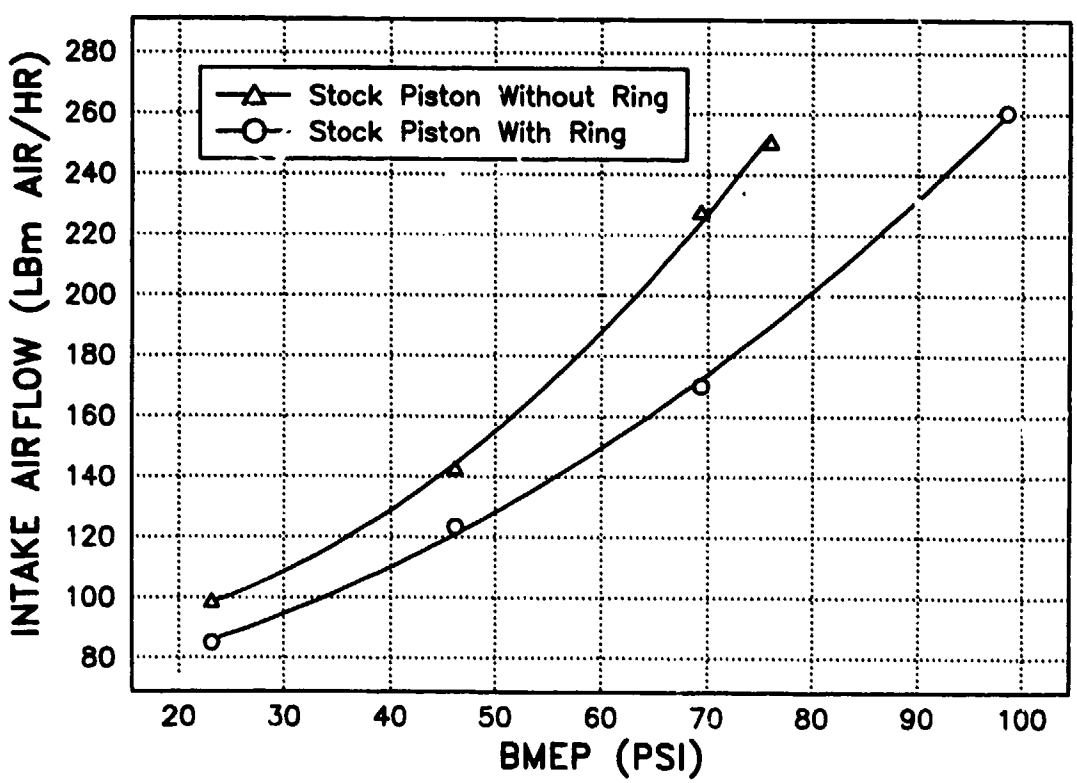

Figure 15. Intake airflow versus brake mean effective pressure for the test engine running with and without the piston ring at 6000 rpm.

The large increase in BSFC for the ringless piston compared to the ringed piston at high loads might also be the result of an increase in piston skirt friction. Piston skirt friction

may increase significantly for the ringless piston during high load operation for two reasons:

(1) The increased blowby at high loads may be blowing or scraping the lubricant off the cylinder wall. A reduction in cylinder wall oil film thickness may result in more metal-to-metal contact and thus friction between the piston and liner.

(2) The hot blowby gas may be heating up the piston skirt, causing a reduction in piston-to-bore clearance. The ringless piston may also become hotter than the ringed piston because there is no piston ring to transfer piston crown heat to the cylinder liner. Thus, the hot running piston-to-bore clearance for the ringless piston may be smaller than the ringed piston clearance, which may result in greater piston skirt friction and lower efficiency for the ringless piston engine.

IV. RINGLESS PISTON DESIGN AND DEVELOPMENT

A joint objective of this project was to design, build and test a piston to improve ringless piston engine performance. Some design considerations for the ringless piston were:

- The piston material must have a thermal expansion coefficient similar to the cast-iron liner to maintain a minimum piston-to-bore clearance over the engine speed/load range (wide piston-liner temperature variation).
- The piston weight must match the stock aluminum piston weight to maintain proper engine balance and produce the same inertial loads on the cylinder wall and crankshaft.
- The piston skirt must have good wear characteristics and be compatible with the cast-iron liner to prevent scuffing and possible seizure.
- The piston must have high strength at elevated temperature to perform in the proposed helicopter compound cycle engine, which operates at high peak cylinder pressures and temperatures.

Based on these design considerations, 4130 steel was selected as the piston material. The thermal expansion coefficient of 4130 steel is $6.3 \times 10^{-6}/^{\circ}F$, which is similar to the cast-iron liner thermal expansion coefficient of $5.6 \times 10^{-6}/^{\circ}F$. The thermal expansion coefficient of aluminum is $12.2 \times 10^{-6}/^{\circ}F$, or more than twice the cast-iron liner coefficient of thermal expansion. The similar coefficients of thermal expansion for the steel piston and cast-iron liner allow tighter fitting of the piston to bore over a given temperature range, as shown in Fig. 16, a plot of piston-to-bore diametrical clearance versus common piston-liner interface temperature. In Fig. 16, it was assumed that the piston and liner remain at the same equilibrium temperature. In reality, a temperature gradient exists between the piston and liner and from top to bottom of each component. The advantage of using a steel piston instead of an aluminum piston in a cast-iron liner is clearly shown in Fig. 16. If an aluminum piston is assembled in a cast-iron liner with an initial clearance of 0.005 inch (0.127 mm), the engine will seize at a component temperature of 350°F (177°C). However, if the aluminum piston is replaced with a steel piston with the same initial clearance, engine seizure will be avoided at 350°F and the final clearance will be reduced by only 0.0005 inch (0.0127 mm). A smaller initial clearance can also be used with the steel piston. As shown in Fig. 16, the initial piston-to-bore clearance for the steel piston in the cast-iron liner can be reduced to 0.001 inch (0.025 mm) without encountering seizure at 350°F (177°C). Thus, using a steel piston in the cast-iron liner will enable the engine to maintain a smaller and more constant piston-to-bore clearance over the engine speed and load range (temperature range). It is very important to maintain a constant minimum piston-to-bore clearance in a ringless engine because this clearance controls the engine power and efficiency.

The 4130 steel also meets the other ringless piston design criteria. Due to the higher strength-to-weight ratio of steel, the steel piston can be made the same weight as the stock aluminum piston. The 4130 steel can be heat-treated to obtain a tensile strength at 480°F (249°C), which is three times greater than aluminum. The steel piston skirt can also be hard chrome-plated for wear resistance and compatibility with the cast-iron liner.

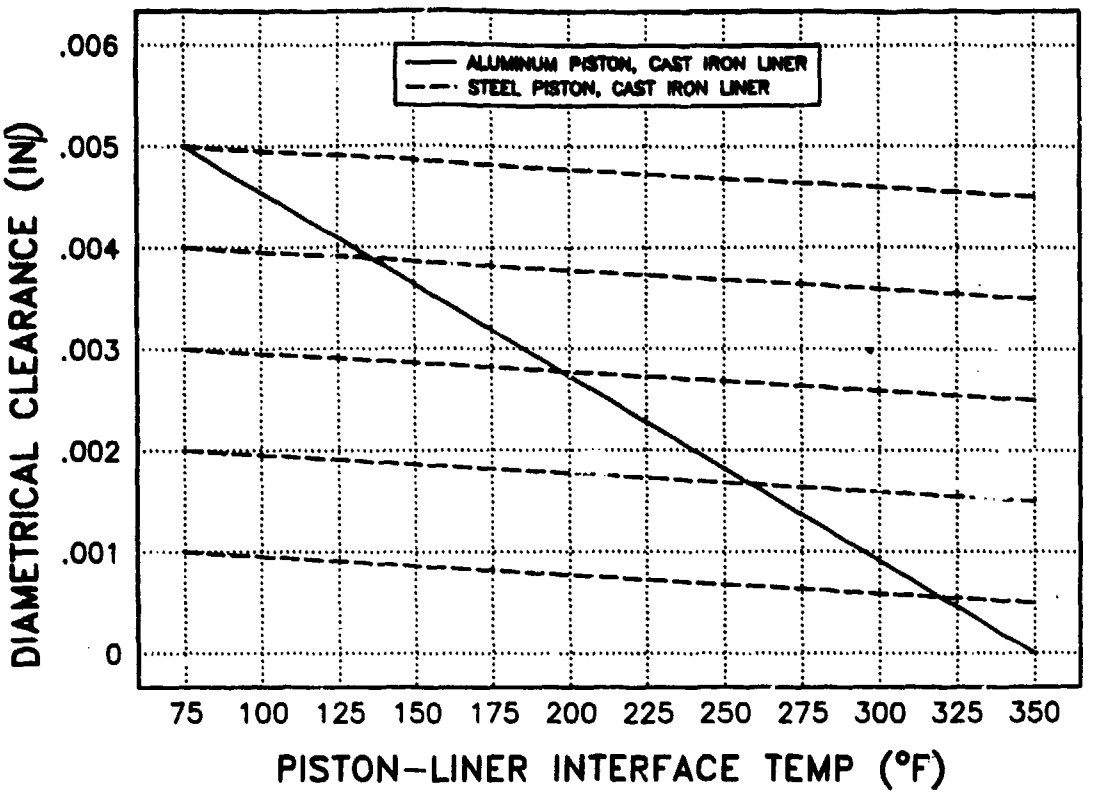

Figure 16. **Piston-to-bore diametrical clearance versus common piston-liner interface temperature for steel and aluminum pistons in the test engine cast-iron liner.**

A. Ringless Steel Piston Fabrication

The steel piston was initially constructed using four components as shown in Fig. 17, a photograph comparing the stock aluminum piston with the prototype steel piston. The steel piston engineering drawing is included in Appendix B. The piston skirt, top, and ring groove were machined from a solid piece of 4130 round stock. The pin boss was machined from steel tubing. The struts used to support the pin bosses were machined out of bar stock steel. The four piston components were furnace-brazed together by microbrazing in a vacuum at 2200°F (1204°C). A section of the steel tubing was removed to allow room for the connecting rod. The piston was then heat-treated and tempered to obtain a Rockwell C-scale hardness of 38 to 42. The piston skirt was hard chrome-plated and ground to obtain a uniform chrome layer 0.002 inch (0.051 mm) thick. The steel piston weighed 206.3 grams versus 212.9 grams for the stock aluminum piston.

The steel piston was designed with a flat top instead of the aluminum piston's dome top as shown in Fig. 18. Fig. 18 compares the front and side views of the steel piston with the stock aluminum piston. The steel piston was designed with a flat top for ease of fabrication despite the fact that a flat-top piston may reduce the squish band, and thus turbulence in the combustion chamber. The flat-top piston reduced the stock compression ratio from 8.4 to 5.6. The stock compression ratio of 8.4 was later obtained with the steel piston by milling the cylinder head. The original compression ratio was not retained by making a taller flat-top piston because a taller piston would contact the cylinder head and affect port timing in the two-stroke engine.

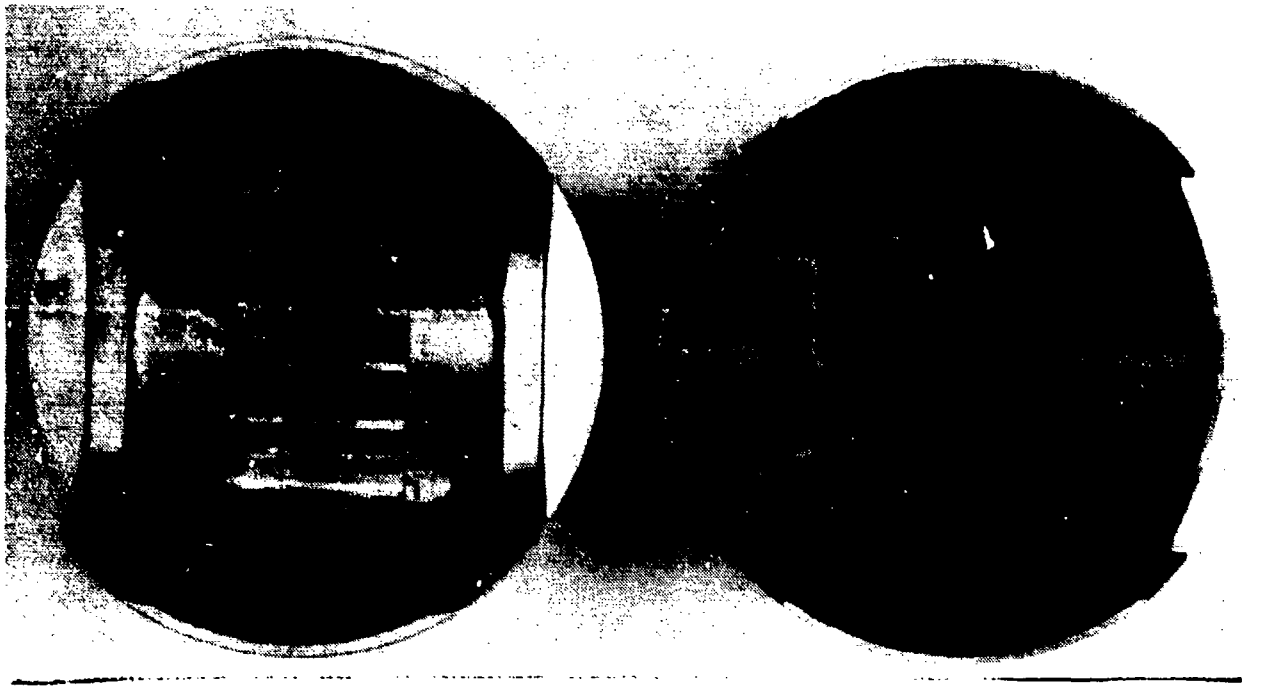

Figure 17. **Photographs comparing the stock aluminum piston (left) with the prototype steel piston (right).**

The piston was designed to minimize piston-to-bore clearance. Therefore, the steel piston was not cam ground. Cam grinding is usually performed to minimize the piston-to-liner contact patch area, which reduces friction. A round piston minimized the area for gas leakage (blowby) between the piston and liner. A round piston should also help to reduce the unit contact stresses between piston and liner and help maintain a maximum oil film thickness to minimize scuffing. Although a temperature gradient exists from the top to the bottom of the piston, the initial steel piston was designed without skirt taper to minimize piston-to-bore clearance.

B. Ringless Steel Piston Tests

The steel piston shown in Figs. 17 and 18 was then tested using the cylinder liner from the previous aluminum piston tests. The cylinder bore and piston diameter measurements used for the first steel piston test are shown in Table 3.

The dimension "TAT" is an acronym for thrust-antithrust and corresponds to the piston and liner dimension perpendicular to the piston pin. The dimension "FB" (Front-to-Back) is the piston and liner dimension measured parallel to the piston pin. The top piston measurement was made just below the ring groove. The middle and bottom piston measurements were made at the piston pin location and bottom of the piston skirt, respectively. The engine was assembled using the steel piston, piston ring and previously used cylinder liner, with the clearances shown in Table 3. The engine started and ran for approximately 30 seconds at 3000 rpm, 20 percent of full load. The engine then seized, causing slight scuffing of the piston and liner. The cause of the seizure was not evident.

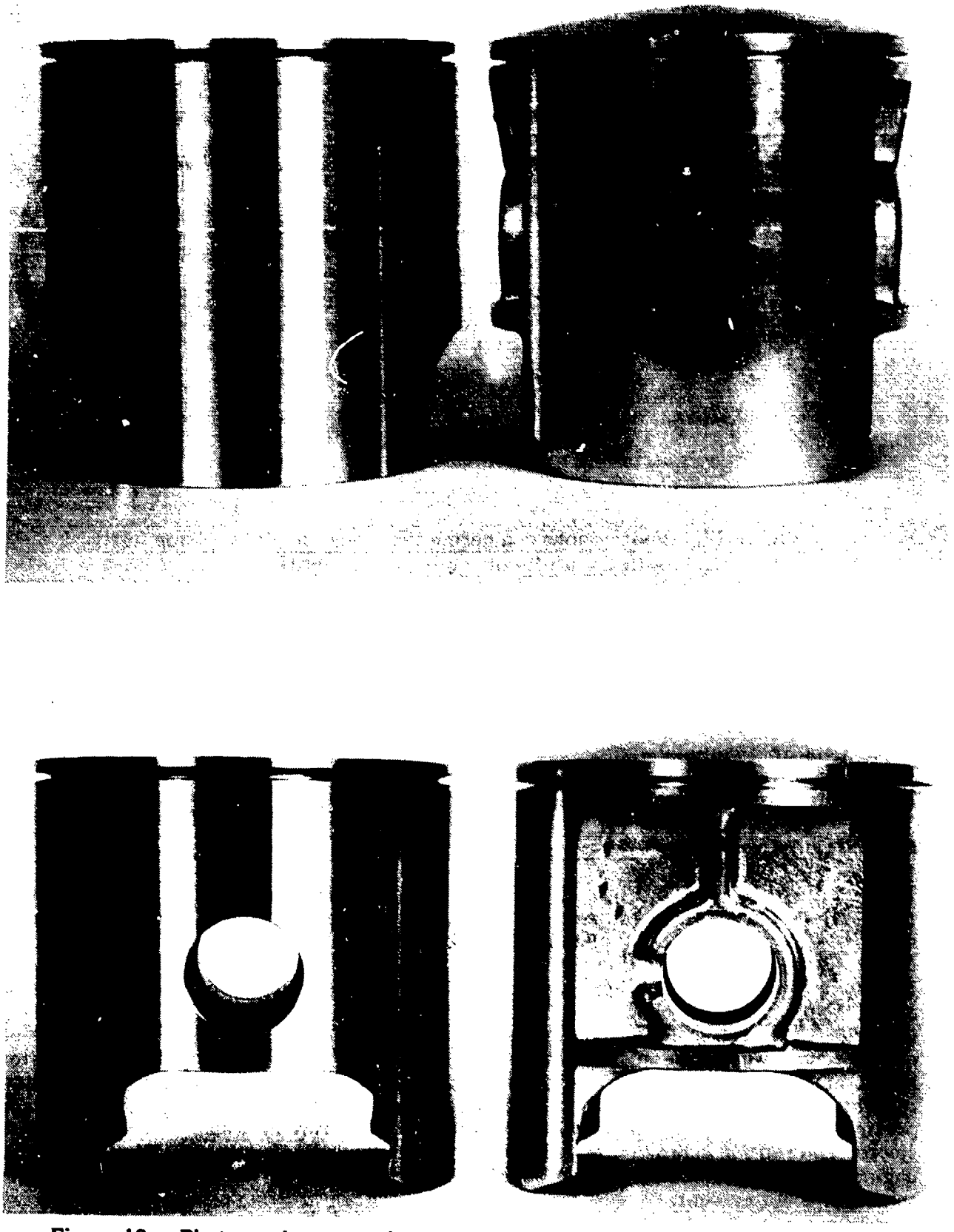

Figure 18. Photographs comparing the front and side views of the prototype steel piston (left) and the aluminum piston (right).

TABLE 3. PISTON AND BORE MEASUREMENTS BEFORE STEEL PISTON TEST NO. 1

	Dimension	Measurement, in.(mm) Top	Middle	Bottom
Cylinder Bore	TAT	2.7569(70.03)	2.7574(70.04)	2.7570(70.03)
	FB	2.7571(70.03)	2.7569(70.03)	2.7575(70.04)
Piston Diameter	TAT	2.7563(70.01)	2.7559(69.99)	2.7559(69.99)
Clearance	TAT	0.0006(0.015)	0.0015(0.04)	0.0011(0.03)

Before the second steel piston test, the cylinder liner was honed to remove scratches and increase the piston-to-bore clearance. Very little damage was done to the steel piston because of the hard chrome plating. The piston scratches were removed, and the piston was polished using fine emery cloth. The piston and cylinder dimensions used for the second steel piston test are given in Table 4.

TABLE 4. PISTON AND BORE MEASUREMENTS BEFORE STEEL PISTON TEST NO. 2

	Dimension	Measurement, in.(mm) Top	Middle	Bottom
Cylinder Bore	TAT	2.7580(70.05)	2.7587(70.07)	2.7584(70.06)
	FB	2.7587(70.07)	2.7589(70.08)	2.7588(70.07)
Piston Diameter	TAT	2.7563(70.01)	2.7567(70.02)	2.7570(70.03)
Clearance	TAT	0.0017(0.04)	0.0020(0.05)	0.0014(0.04)

The engine was assembled, and the carburetor main jet was increased from No. 320 to No. 330 to provide more cylinder lubrication. The engine started and ran well at 3000 rpm. However, at 4000 rpm the engine load began to drop as the throttle was opened. The engine was shut down to prevent another seizure. The engine was torn down and the measurements taken as shown in Table 5. The carburetor main jet was changed back to the original No. 320.

The piston was out-of-round by 0.0026 inch (0.0660 mm). The steel piston had grown parallel to the piston pin, indicating that the piston thrust load was causing piston flexure.

TABLE 5. PISTON AND BORE MEASUREMENTS AFTER STEEL PISTON TEST NO. 2

	Dimension	Measurement, in.(mm) Top	Middle	Bottom
Cylinder Bore	TAT	2.7580(70.05)	2.7587(70.07)	2.7584(70.06)
	FB	2.7587(70.07)	2.7589(70.08)	2.7588(70.07)
Piston Diameter	TAT	2.7564(70.01)	2.7561(70.00)	2.7567(70.02)
	FB	-	2.7535(69.94)	-
Clearance	TAT	0.0016(0.04)	0.0026(0.07)	0.0019(0.05)
	FB	-	0.0054(0.14)	-

The steel piston was then pressed back into shape and a file was used to remove high spots. The cylinder liner was also honed. The piston and bore dimensions used for the third steel piston test are shown in Table 6.

TABLE 6. PISTON AND BORE MEASUREMENTS BEFORE STEEL PISTON TEST NO. 3

	Dimension	Measurement, in.(mm) Top	Middle	Bottom
Cylinder Bore	TAT	2.7599(70.10)	2.7599(70.10)	2.7599(70.10)
	FB	2.7605(70.12)	2.7602(70.11)	2.7599(70.10)
Piston Diameter	TAT	2.7562(70.00)	2.7560(70.00)	2.7561(70.02)
	FB	-	2.7529(69.92)	-
Clearance	TAT	0.0037(0.093)	0.0039(0.099)	0.0038(0.0965)
	FB	-	0.0073(0.185)	-

The engine was assembled and again ran well at 3000 rpm, but began to seize at 4000 rpm. The piston was removed and found to be out-of-round as before. Apparently, at engine speeds greater than 3000 rpm, the piston inertia forces were causing the piston skirt to distort and cause seizure.

The steel piston was then modified by soldering in a doughnut-shaped piston strut. The strut increased the steel piston weight from 206.3 to 212.9 grams. The strut was furnace-brazed in place using a high silver content solder at 500°F (260°C). The piston strut was placed inside the piston just below the piston pin and parallel to the piston top. The outside diameter of the strut was used to keep the piston skirt round. The engine connecting rod passed through the center of the doughnut-shaped strut. The engine was then assembled with the piston-to-bore clearances shown in Table 7.

TABLE 7. PISTON AND BORE MEASUREMENTS BEFORE STEEL PISTON TEST NO. 4

	Dimension	Measurement, in.(mm) Top	Middle	Bottom
Cylinder Bore	TAT	2.7599(70.10)	2.7599(70.10)	2.7599(70.10)
	FB	2.7506(69.87)	2.7602(70.11)	2.7599(70.10)
Piston Diameter	TAT	2.7562(70.00)	2.7577(70.05)	2.7599(70.10)
	FB	-	2.7572(70.03)	-
Clearance	TAT	0.0037(0.093)	0.0022(0.0559)	0.0014(0.0356)
	FB	-	0.0027((0.068)	-

The engine ran well at 3000 rpm, but began to seize again at 4000 rpm. The liner was honed again to increase the piston-to-bore clearance and the engine was assembled with the dimensions shown in Table 8.

TABLE 8. PISTON AND BORE MEASUREMENTS BEFORE STEEL PISTON TEST NO. 5

	Dimension	Measurement, in.(mm) Top	Middle	Bottom
Cylinder Bore	TAT	2.7620(69.09)	2.7622(70.16)	2.7630(70.18)
	FB	2.7619(70.15)	2.7621(70.16)	2.7639(70.20)
Piston Diameter	TAT	2.7550(69.98)	2.7574(70.04)	2.7579(70.05)
	FB	-	2.7574(70.04)	-
Clearance	TAT	0.007(0.1778)	0.0048(0.1219)	0.0051(0.130)
	FB	-	0.0047(0.1193)	-

The engine was assembled as before with the piston ring and ran well at 3000, 4000, and 5000 rpm. At 6000 rpm, the higher piston temperature caused the solder that was holding the doughnut-shaped strut in place to fail. The strut came loose in the engine and was sheared into several pieces by the piston passing over the transfer ports. The engine had to be removed from the test stand and completely disassembled to remove metal filings from the engine crankcase.

The first steel piston was used as a sacrificial development tool. It was obvious from the initial steel piston test results that skirt flexure occurred at speeds greater than 3000 rpm. The piston skirt deformation caused the piston to seize in the cylinder. The steel piston also had a tendency to scuff near the top of the piston, indicating that the piston

should be tapered to account for the temperature gradient between the top and bottom of the piston.

The steel piston was then modified to incorporate the knowledge gained during the first steel piston tests. The piston was dechromed and new piston skirt support struts were designed and fabricated. The engineering drawing for the new struts is given in Appendix B. Two support struts were furnace-brazed in the piston at 2200°F (1204°C) using the original piston solder. Each strut was located perpendicular to the piston pin, as shown in Figs. 19 and 20. (Previously, the doughnut-shaped strut was furnace-brazed in the piston at 500°F (260°C) to avoid having to dechrome and reheat-treat the piston.) The steel piston was then heat-treated in a special fixture to prevent the piston from warping. The piston skirt was plated with a 0.006-inch (0.152-mm) thick layer of chrome. A 0.002-inch (0.051-mm) taper was then ground into the piston skirt from the top of the piston to the piston pin hole. Adding the two support struts and extra chrome plating increased the weight of the steel piston from 206.3 to 246.0 grams, or a 19 percent increase.

The engine was then assembled using the modified steel piston and a new cylinder liner. The piston and bore measurements are given in Table 9.

The engine was assembled without the piston ring to ensure that ringless engine data would be collected. The chance of getting ringless piston performance data would be reduced if the engine seized during ringed tests. Also, the temperature profile of a ringless piston is different from a ringed piston because there is no ring to conduct heat from the piston crown to the cylinder wall. Therefore, it made more sense to optimize the piston-to-bore clearance and piston geometry of the ringless piston because the ringless steel piston data were most important.

The ringless steel piston was assembled with a smaller piston-to-bore clearance than the ringless aluminum piston because of the steel's lower coefficient of thermal expansion. During the project, the engine was hand-cranked with the aluminum and steel ringless pistons. The ringless steel piston engine had much higher compression pressure than the ringless aluminum piston.

The engine started immediately with the ringless steel piston. (The ringless aluminum piston usually required approximately 5 to 10 seconds for the combustion gases to heat the piston and reduce the clearance before the engine would run.) The engine ran fine at 3000 rpm low load, but seized at full load. The piston seized just below the ring groove, as shown in Figs. 21 and 22. A shiny ring was formed all the way around the piston just below the ring groove, indicating that metal-to-metal contact had occurred. The steel piston also had some shiny spots on its antithrust side (Fig. 21) where it appeared that the edge of the exhaust port was contacting the piston. A small shiny spot was also evident on the thrust side of the piston skirt, as shown in Fig. 22. Fig. 22 shows that the thrust side of the piston skirt was making metal-to-metal contact with a thin section of cylinder liner located between the intake ports.

The steel piston was removed from the engine and the piston taper from the piston pin hole to the top of the piston was increased by 0.0015 inch (0.038 mm). The cylinder liner was gently massaged with fine emery cloth to remove scratches. The piston-to-bore clearance of 0.0015 inch (0.038 mm) had worked well at 3000 rpm, but more piston taper was required for higher load operation.

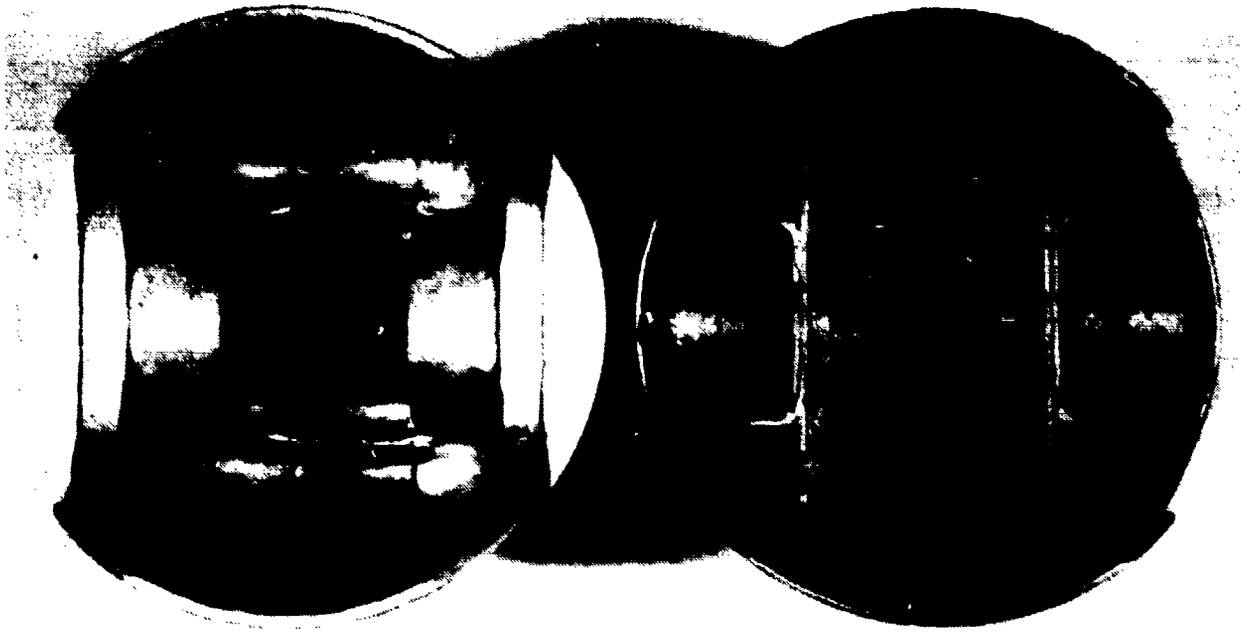

Figure 19. Photographs showing comparison between new steel piston with support struts (right) with stock aluminum piston (left).

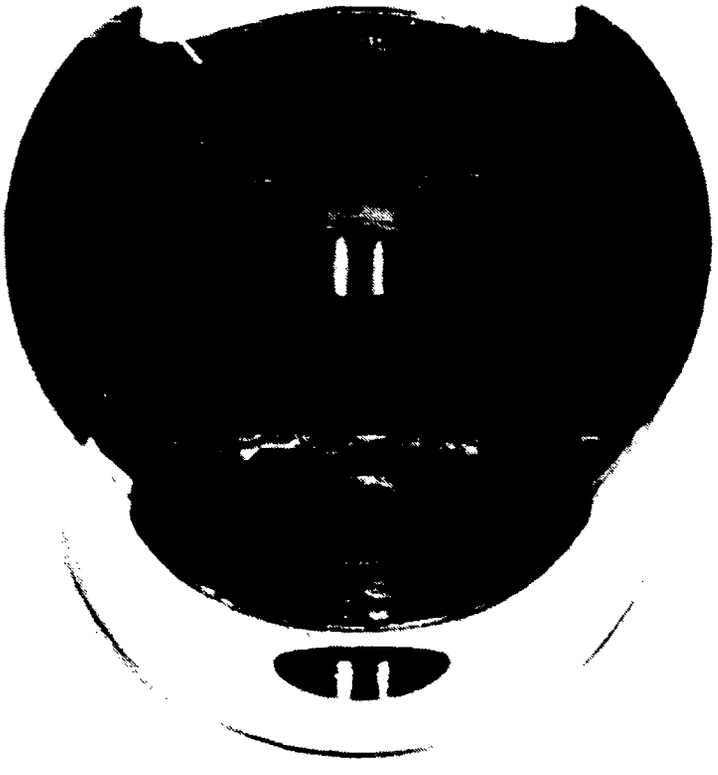

Figure 20. Photograph showing steel piston support struts.

TABLE 9. PISTON AND BORE MEASUREMENTS BEFORE STEEL PISTON TEST NO. 6

	Dimension	Measurement, in.(mm) Top	Middle	Bottom
Cylinder Bore	TAT	2.7565(70.01)	2.7565(70.01)	2.7565(70.01)
	FB	2.7565(70.01)	2.7565(70.01)	2.7565(70.01)
Piston Diameter	TAT	2.7535(69.94)	2.7550(69.98)	2.7550(69.98)
	FB	2.7535(69.94)	2.7550(69.98)	2.7550(69.98)
Clearance	TAT	0.0035(0.089)	0.0015(0.038)	0.0015(0.038)

Figure 21. Photograph of modified steel piston after steel piston test No. 6 showing the metal-to-metal contact that occurred just below the ring groove and on the antithrust side of the piston.

Figure 22. Photograph of modified steel piston after steel piston test No. 6 showing the metal-to-metal contact that occurred just below the ring groove and on the thrust side of the piston.

The engine was assembled with the piston and bore measurements shown in Table 10.

TABLE 10. PISTON AND BORE MEASUREMENTS BEFORE STEEL PISTON TEST NO. 7

	Dimension	Measurement, in.(mm) Top	Middle	Bottom
Cylinder Bore	TAT	2.7565(70.01)	2.7565(70.01)	2.7565(70.01)
	FB	2.7565(70.01)	2.7565(70.01)	2.7565(70.01)
Piston Diameter	TAT	2.7520(69.90)	2.7550(69.98)	2.7550(69.98)
	FB	2.7520(69.90)	2.7550(69.98)	2.7550(69.98)
Clearance	TAT	0.0045(0.114)	0.0015(0.038)	0.0015(0.038)

The extra clearance at the top of the piston allowed the engine to run at 3000 rpm full load. At 4000 rpm, however, the engine load began to drop as the throttle was opened, indicating that seizure was about to occur. The piston was removed and inspected. Metal-to-metal contact was still taking place just below the ring groove, as shown in Figs. 21 and 22. The piston taper was increased by another 0.0015 inch (0.038 mm), and the engine was assembled with the measurements shown in Table 11.

TABLE 11. PISTON AND BORE MEASUREMENTS BEFORE STEEL PISTON TEST NO. 8

	Dimension	Measurement, in.(mm) Top	Middle	Bottom
Cylinder Bore	TAT	2.7565(70.01)	2.7565(70.01)	2.7565(70.01)
	FB	2.7565(70.01)	2.7565(70.01)	2.7565(70.01)
Piston Diameter	TAT	2.7505(69.86)	2.7550(69.98)	2.7550(69.98)
	FB	2.7505(69.86)	2.7550(69.98)	2.7550(69.98)
Clearance	TAT	0.0060(0.1524)	0.0015(0.038)	0.0015(0.038)

The engine started and ran well between speeds of 3000 and 6000 rpm. There was no evidence of piston seizure. The new piston struts eliminated the problem of piston skirt flexure. The final steel piston taper of 0.006 inch (0.152 mm) was larger than the taper originally thought to be required. The stock aluminum piston uses a taper of 0.007 inch (0.178 mm). It was anticipated that the steel piston would require a smaller taper because the coefficient of thermal expansion for steel is less than half of the aluminum value. This result suggests that the ringless piston operating temperature must be significantly higher than the ringed aluminum piston operating temperature. Evidence for the high steel piston temperature is shown in Fig. 23, which is a photograph of the steel piston top after steel piston test No. 8. The light blue and straw colors indicate that the piston temperature was 525° (274°) and 450°F (232°C), respectively, at the location of these two colors.

Four possible explanations for the high ringless steel piston temperature are:

(1) The thermal conductivity of steel is approximately one-third that of aluminum.

(2) The ringless piston has no ring to conduct heat from its crown to the cylinder liner.

(3) The blowby gas may be heating up the piston.

(4) The ringless steel piston does not have cooling fins on the underside of its crown, as shown in Figs. 17 and 19.

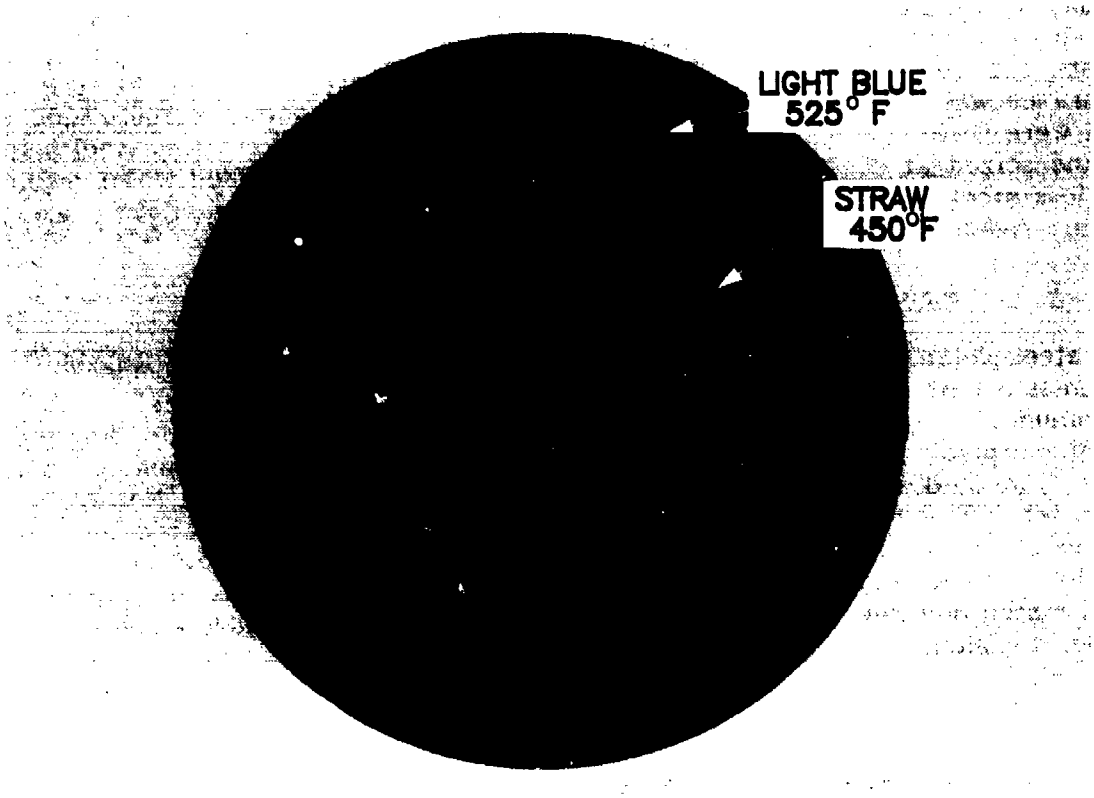

Figure 23. Photograph showing the temperatures on the steel piston crown.

C. Ringless Steel Piston Test Procedure

Before conducting the steel piston tests, a new baseline maximum power performance test was conducted with the ringed aluminum piston. A new baseline data set was required because the ambient test cell temperature had increased by 30°F (16.7°C) since the previous baseline test. The carburetor main jet had to be reduced from a No. 320 to a No. 310 to adjust the full load air-fuel ratio. The results of the new baseline test are given in Table A-3 of Appendix A. The maximum power curve for the new baseline test is lower than that of the original baseline power curve due to the use of a smaller carburetor main jet.

The steel piston was then tested without the piston ring so that ringed aluminum piston and ringless steel piston engine performance could be compared. The steel piston was not tested with a ring because the steel piston taper and piston-to-bore clearance had been optimized for ringless piston operation. The ringless steel piston was tested with the dimensions and clearances listed in table 11. The assembled compression ratio for the flat-topped steel piston was 5.6 compared to the stock aluminum piston compression ratio of 8.4. Full load data points were recorded at 3000, 4000, and 6000 rpm. The engine seized at 7000 rpm before a data point could be recorded. A data point at 5000 rpm was not recorded due to engine operator error.

The engine was disassembled and inspected. The piston had made metal-to-metal contact with the cylinder just above the ends of the piston pin. The cylinder liner was gently massaged with emery cloth to remove scratches. The piston was also sanded where metal-to-metal contact had occurred to remove scratches and slightly increase

the piston-to-bore clearance. The cylinder head was modified to reduce the clearance volume and increase the compression ratio from 5.6 to the stock value of 8.4 with the flat-topped steel piston. The engine was assembled with the ringless steel piston. The clearances were the same as shown in Table 11 except the top FB piston-to-bore clearance was increased by 0.0005 inch (0.013 mm). Data points at 3000, 4000, and 5000 rpm were recorded with the standard compression ratio (8.4) ringless steel piston. The engine seized at 6000 rpm before a data point could be recorded. The results of the ringless steel piston performance tests with an 8.4:1 compression ratio are given in Table A-4 in Appendix A.

D. Ringless Steel Piston Performance Results

The steel piston and stock aluminum piston power ratio curves are compared in Fig. 24, which is a plot of power ratio versus engine speed for the three test conditions. The aluminum piston power ratio curve (shown earlier) was generated by dividing the ringless aluminum piston power by the ringed aluminum piston power. The aluminum piston tests were conducted with the stock compression ratio of 8.4 and using a No. 320 carburetor main jet. The two steel piston power ratio curves were generated by dividing the ringless steel piston power obtained with compression ratios of 5.6 and 8.4 by a new baseline ringed aluminum piston power using the stock compression ratio of 8.4. The steel piston and new aluminum piston baseline tests were conducted with a No. 310 carburetor main jet.

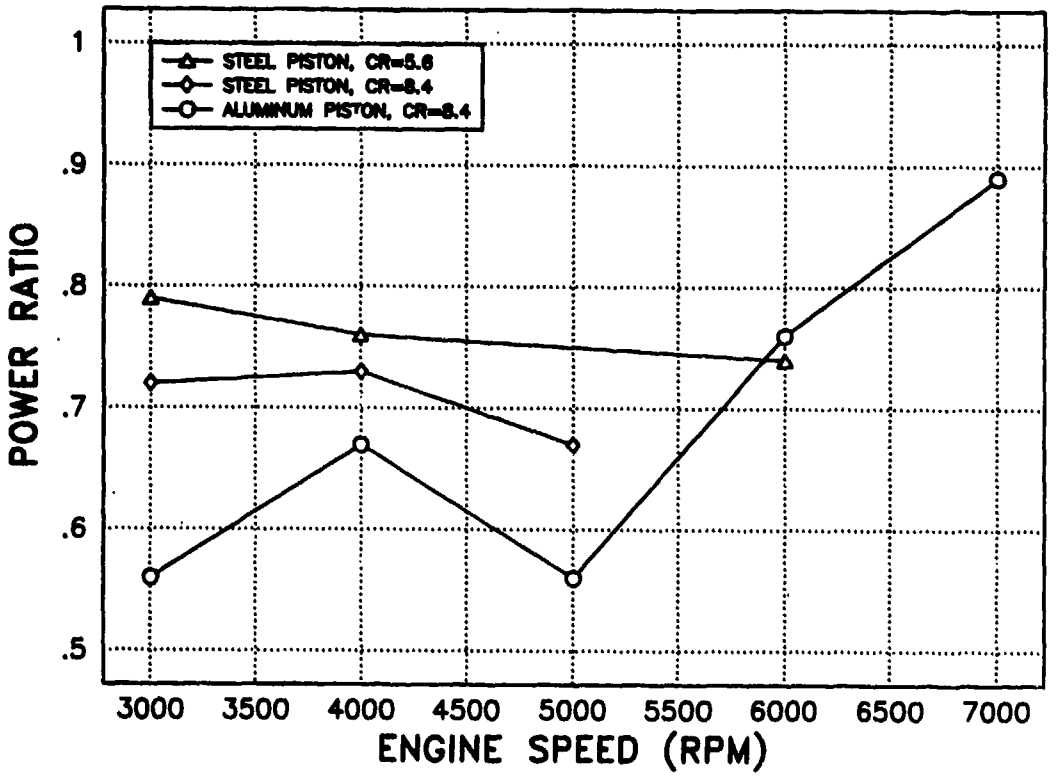

Figure 24. Power ratio versus engine speed for the Suzuki engine comparing the results of the ringless aluminum piston and ringless steel piston at compression ratios of 5.6 and 8.4.

The curves in Fig. 24 show that the steel piston power ratio was significantly higher than the aluminum piston power ratio at engine speeds below 6000 rpm. For example, at 3000 rpm the power ratio increased by 37 percent for the steel piston (CR = 5.6) compared to the stock aluminum piston. The increase in power ratio was attributed to the smaller initial piston-to-bore clearance for the steel piston (0.0015 inch) (0.0381 mm) compared to the aluminum piston clearance of 0.0033 inch (0.0838 mm). The steel piston (CR = 5.6) power ratio was 10 percent higher at 4000 rpm. However, at 6000 rpm the steel piston power ratio was 4 percent lower than the aluminum piston power ratio. The lower steel piston power ratio was probably due to increased friction associated with the reduced clearance at 6000 rpm.

The power ratio for the steel piston at the 8.4 compression ratio was also improved relative to the stock aluminum piston power ratio. Power ratio increases of 27, 7, and 20 percent were measured at engine speeds of 3000, 4000, and 5000 rpm, respectively. The improved power ratio was again attributed to the steel piston's smaller piston-to-bore clearance.

The smaller piston-to-bore clearance for the steel piston resulted in reduced blowby for the steel ringless piston compared to the aluminum ringless piston. Evidence for the reduced steel piston blowby is shown in Fig. 24. Fig. 25 is a photograph comparing the steel piston with the aluminum piston after ringless piston operation. The aluminum piston is discolored below the ring groove where the blowby gases left oil deposits. There was no evidence of blowby deposits below the ring groove with the steel piston.

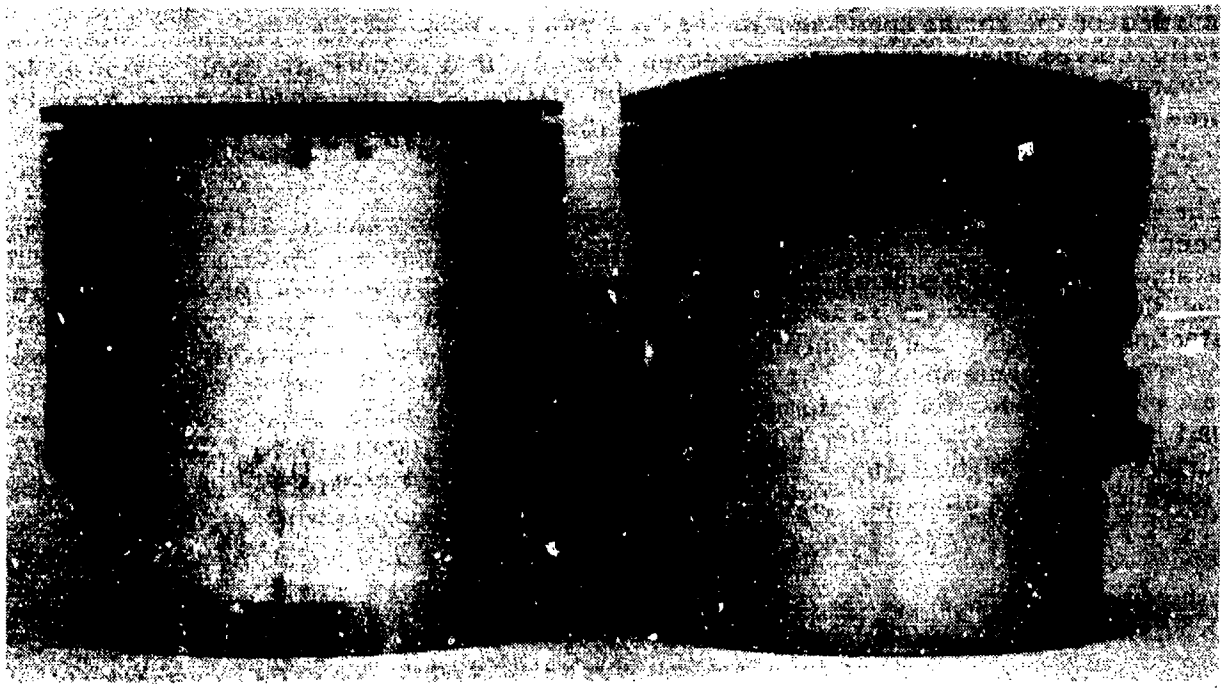

Figure 25. Photograph comparing the prototype steel piston (left) and aluminum piston (right) after ringless operation followed by seizure at 7000 rpm.

The improved durability of the steel piston versus the aluminum piston is also shown in Fig. 25. Fig. 25 shows the thrust side of the steel and aluminum pistons after both pistons seized at 7000 rpm. The chrome-plated steel piston was not seriously damaged and could be run again after polishing the chrome surface. The aluminum piston was severely damaged and had to be replaced. Aluminum had transferred from the piston to the cylinder wall.

The curves in Fig. 24 also show that the power ratio decreased for the steel piston when the compression ratio was increased from 5.6 to 8.4. The power ratio decreased by 9 and 3 percent at engine speeds of 3000 and 4000 rpm, respectively. This power ratio decrease could be due to several factors. First, as shown in Fig. 3, the power ratio decreases with increasing compression ratio. However, it was expected that the power ratio would increase slightly with increasing compression ratio due to improved thermal efficiency. The power ratio decrease may also be the result of modifying the two-stroke engine's combustion chamber. Approximately 0.125 inch (3.175 mm) had to be milled off the cylinder head to increase the compression ratio from 5.6 to 8.4. This modification removed most of the combustion chamber squish band, which may have adversely affected engine performance. The reduced power ratio may also be attributed to the higher cylinder gas pressures and temperatures. The higher temperatures may have increased engine friction by reducing the piston-to-bore clearance.

The slopes of the steel and aluminum piston power ratio curves are different, as shown in Fig. 24. The aluminum piston curve increases with engine speed, indicating that the piston-to-bore clearance changes significantly over the engine speed and load range. The slope of the steel piston power ratio curve is slightly negative and approximately five times lower than the slope of the aluminum piston power ratio curve. The smaller slope for the steel piston curves indicates that the piston-to-bore clearance does not change much over the engine speed and load range. The negative slope of the steel piston power ratio curves may be due to increased friction that occurs at small piston-to-bore clearances. The negative slope may also be attributed to the steel piston's 20 percent weight increase over the stock aluminum piston. The heavier steel piston may cause higher piston inertial thrust loads and increased friction.

The slope and magnitude of the steel and aluminum piston power ratio curves may have been changed by starting out with different initial piston-to-bore clearances. For example, if a larger initial piston-to-bore clearance had been used for the steel piston, the slope of the power ratio curve may have increased with engine speed. However, starting out with a larger initial clearance would have reduced the steel piston power ratio at low engine speeds. The slope may have reduced and the power ratio increased at low engine speeds for the aluminum piston if a smaller initial piston-to-bore clearance had been used. The smaller initial clearance, however, would have resulted in engine seizure at the higher engine speeds because of the large change in the piston-to-bore clearance for the aluminum piston.

V. COMPARISON OF ANALYTICAL AND EXPERIMENTAL ENGINE PERFORMANCE RESULTS

Fig. 26 is a plot of power ratio versus engine speed that compares the maximum power performance results of the engine model with the experimental data shown in Fig. 24. The three smooth curves shown in Fig. 26 are the result of the computer simulation of a ringless piston for piston-to-bore diametrical clearances of 0.001 (0.025), 0.002 (0.051) and 0.003 (0.076) inch (mm). It is important to realize that the experimental data shown in Figs. 24 and 26 include the effect of engine speed, piston-to-bore clearance, friction, and combustion on the engine power ratio. The engine model accounts for changes in engine speed and piston-to-bore clearance but does not include the effects of friction and combustion on engine power ratio.

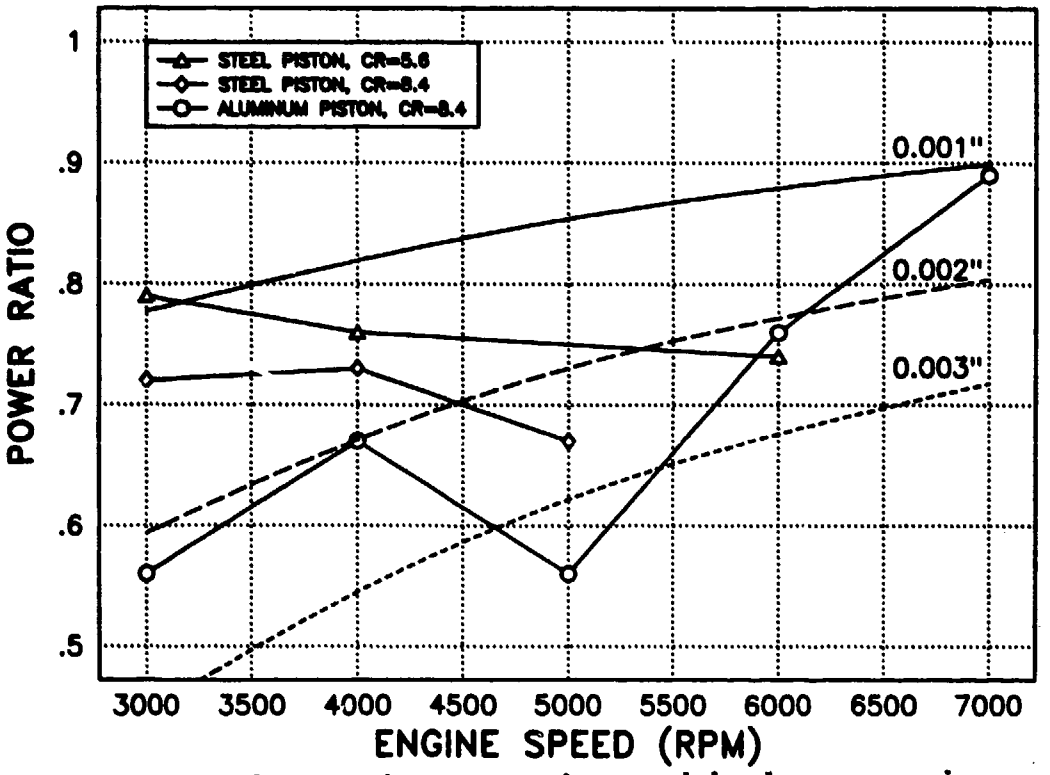

Figure 26. **Power ratio versus engine speed showing a comparison between the engine model and the aluminum steel piston experimental data.**

The aluminum piston data will first be compared with the engine model results. The aluminum piston data and engine model both show that the power ratio increases with engine speed (except for the data point at 5000 rpm discussed earlier in this report). The power ratio increases with engine speed because there is less time per engine cycle for the combustion gas to leak past the piston. The piston-to-bore clearance becomes smaller at high engine speeds and loads due to the increased piston temperature. The reduction in piston-to-bore clearance can be seen in Fig. 26 by comparing the aluminum piston experimental data with the engine model results. As the engine speed (and thus load at this full power condition) increases, the aluminum piston power ratio increases in the direction of reduced piston-to-bore clearance, as shown in Fig. 26.

The steel piston performance results are also shown in Fig. 26. By comparing the steel piston results with the engine model, it appears that the steel piston piston-to-bore clearance actually increases with engine speed due to the reduction in power ratio. The reduction in power ratio, however, was not due to increased clearance but increased friction at a reduced clearance. The steel piston data may have shown the same trend as the aluminum piston data and engine model results if a larger initial piston-to-bore clearance had been used.

The experimental results show that there is an optimum piston-to-bore clearance where the increase in engine performance due to reduced blowby is no longer greater than the decrease in engine performance due to increased friction.

A major challenge for the ringless engine is to design an engine with constant minimum piston-to-bore clearance over the engine speed and load range. This could be accomplished using piston and liner materials with similar coefficients of thermal expansion, if the piston and liner remain at the same temperature. However, a temperature gradient exists between these two components that is a function of engine speed and load. Potential solutions to this problem would be either to run the engine at constant speed and load or to use variable piston and liner cooling to maintain a constant piston-to-bore clearance.

Conventional engines are typically designed with piston and cylinder assemblies that are thermally unstable. For example, most pistons are made of a material that expands at a faster rate than the cylinder liner. When the engine load (temperature) increases, the piston expands more than the liner, resulting in piston seizure. Even pistons and liners made of the same material have a tendency to seize because the piston temperature increases faster than the cylinder liner temperature. To prevent engine seizure, a thermally stable piston cylinder assembly is required. The liner should be made of a material that has a higher coefficient of thermal expansion compared to the piston material. If the engine were overheated with a thermally stable piston cylinder assembly, the blowby would increase and piston seizure would be prevented. The thermally stable piston cylinder assembly would act as a control system to prevent engine seizure. Model airplane engines that operate without rings at very high speeds use this technique to prevent piston seizure.

VI. CONCLUSIONS AND RECOMMENDATIONS

The following conclusions were made based upon this investigation.

- Ringless piston engine power and efficiency are defined by the expression C/NBS, where

  C = Piston-to-bore diametrical clearance
  N = Engine speed in rpm
  B = Engine bore
  S = Engine stroke

- Engine power and efficiency are maximized when the expression C/NBS is minimized.

- Blowby in a ringless piston engine increases with compression ratio.

- A ringless piston engine should be designed with piston and liner materials that have similar coefficients of thermal expansion.

- Ringless piston engine performance can be improved by using a steel piston in a cast-iron liner in place of an aluminum piston in a cast-iron liner. A chrome-plated steel piston has the following advantages over an aluminum piston:

  -- The steel piston has higher strength at elevated temperatures.
  -- A chrome-plated steel piston resists scuffing and is more durable.
  -- A smaller and more constant piston-to-bore clearance can be obtained with a steel piston. The reduced clearance results in improved engine power, efficiency, and cold starting.

The following recommended work should be conducted using the test rig manufactured by AVL located in the SwRI Fuels and Lubricants Research Division. The AVL test rig is currently being assembled at SwRI to conduct further compound cycle engine development.

- Labyrinth seals should be investigated as an alternate method of sealing the piston in the cylinder. Labyrinth seals should be modeled and tested to determine their effect on ringless piston engine performance.

- Other piston and liner materials should be evaluated and tested to determine their potential for ringless piston operation. A thermally stable engine (liner expands faster than the piston) could be constructed using a titanium piston in a cast-iron or chrome oxide-coated aluminum liner. Other researchers (3) have had good success using monolithic ceramic pistons and liners for ringless piston operation.

- Motoring engine friction tests should be conducted to compare conventional engine friction (engines using conventional piston-to-bore clearances and rings) with ringless piston engine friction using reduced piston-to-bore clearances.

- An air bearing between the piston and liner should be investigated as a potential means of reducing piston/liner wear in the compound cycle engine. The engine geometry required to create an air bearing between the piston and liner should be determined as a function of engine bore, stroke, speed, and piston-to-bore clearance.

VIII. LIST OF REFERENCES

1. Executive Summary, Compound Cycle Engine for Helicopter Application, Contract No. NAS3-24346 21-5854, Garrett Turbine Engine Company, Phoenix, Arizona, prepared for U.S. Army Aviation Systems Command and National Aeronautics and Space Administration, Cleveland, Ohio, 1 April 1986.

2. Lilly, L. R. C., Diesel Engine Reference Book, London, England, Butterworths and Co., Ltd., 1984.

3. Wade, W. R., A Structural Ceramic Diesel Engine - The Critical Elements, Ford Motor Company, Dearborn, Michigan.

TABLE A-1. RINGED ALUMINUM PISTON PERFORMANCE DATA
No. 320 CARBURETOR MAIN JET, COMPRESSION RATIO = 8.4

Engine Speed (rpm)	Power Output (Bhp)	% Load	BMEP (psi)	Air-flow (lb/hr)	Fuel Flow (lb/hr)	Air/ Fuel	BSFC (lb fuel/ hp-hr)	Intake Air Temp (°F)	Exhaust Gas Temp (°F)
3000	1.7	25	15.2	46.94	4.72	9.95	2.72	65	286
3000	3.4	50	30.2	55.91	5.42	10.31	1.57	64	402
3000	5.2	75	45.4	76.72	6.58	11.65	1.27	65	455
3000	6.4	100	56.1	105.08	10.06	10.45	1.57	64	471
4000	2.0	25	13.3	59.81	6.33	9.44	3.14	65	396
4000	4.0	50	26.3	73.65	7.57	9.73	1.89	65	480
4000	6.0	75	39.6	90.73	9.06	10.01	1.50	64	526
4000	8.5	100	55.8	134.45	16.06	8.37	1.89	65	558
5000	3.2	25	16.6	63.54	6.48	9.80	2.06	65	504
5000	6.3	50	33.1	76.75	7.38	10.41	1.17	65	584
5000	9.5	75	49.7	102.73	10.30	9.98	1.09	65	624
5000	12.2	100	63.7	171.56	18.75	9.15	1.54	65	597
6000	5.3	25	23.2	85.28	8.58	9.93	1.62	66	651
6000	10.6	50	46.2	123.52	11.76	10.50	1.12	65	725
6000	15.8	75	69.4	170.21	15.88	10.72	1.00	65	771
6000	22.2	100	97.3	260.73	29.26	8.91	1.32	65	725
7000	7.4	25	27.9	--	--	--	--	66	--
7000	14.8	50	55.6	137.76	11.50	11.98	0.78	66	753
7000	22.2	75	83.4	202.99	22.33	9.09	1.00	66	852
7000	29.3	100	111.1	288.92	31.93	9.05	1.09	66	835

TABLE A-2. RINGLESS ALUMINUM PISTON PERFORMANCE DATA
No. 320 CARBURETOR MAIN JET, COMPRESSION RATIO = 8.4

Engine Speed (rpm)	Power Output (Bhp)	% Load	BMEP (psi)	Air-flow (lb/hr)	Fuel Flow (lb/hr)	Air/ Fuel	BSFC (lb fuel/ hp-hr)	Intake Air Temp (°F)	Exhaust Gas Temp (°F)
3000	1.7	25	15.2	60.43	5.51	10.96	3.18	54	377
3000	3.4	50	30.2	103.80	9.78	10.62	2.83	54	424
3000	3.6	max	32.0	110.50	10.19	10.84	2.83	54	422
4000	2.0	25	13.3	67.77	7.06	9.60	3.50	54	446
4000	4.0	50	26.3	86.24	8.15	10.59	2.03	54	489
4000	5.9	max	39.4	139.34	15.86	8.78	2.70	54	494
5000	3.2	25	16.6	74.43	8.06	9.24	2.56	54	550
5000	6.3	50	33.1	170.36	19.31	8.82	3.06	55	516
5000	6.9	max	36.2	180.19	20.03	8.99	2.90	54	506
6000	5.3	25	23.2	99.04	9.61	10.31	1.81	55	660
6000	10.6	50	46.2	142.83	12.72	11.23	1.21	54	704
6000	15.8	75	69.4	227.83	25.89	8.80	1.63	54	647
6000	17.0	max	74.7	250.91	29.50	8.50	1.74	55	632
7000	26.1	max	98.0	--	--	--	--	55	--

TABLE A-3. RINGED ALUMINUM PISTON PERFORMANCE DATA
No. 310 CARBURETOR MAIN JET, COMPRESSION RATIO = 8.4

Engine Speed (rpm)	Power Output (Bhp)	% Load	BMEP (psi)	Air-flow (lb/hr)	Fuel Flow (lb/hr)	Air/ Fuel	BSFC (lb fuel/ hp-hr)	Intake Air Temp (°F)	Exhaust Gas Temp (°F)
3000	6.0	100	52.4	97.12	9.20	10.56	1.54	95	468
4000	7.4	100	50.0	131.74	14.71	8.95	1.92	95	556
5000	9.2	100	48.4	153.47	17.31	8.87	1.88	95	641
6000	18.6	100	81.6	241.39	26.75	9.02	1.44	95	719
7000	28.5	100	107.1	--	--	--	--	95	--

TABLE A-4. RINGLESS STEEL PISTON PERFORMANCE DATA WITH COMPRESSION RATIOS OF 5.6 AND 8.4 No. 310 CARBURETOR MAIN JET

Compression Ratio = 5.6

Engine Speed (rpm)	Power Output (Bhp)	% Load	BMEP (psi)	Air-flow (lb/hr)	Fuel Flow (lb/hr)	Air/ Fuel	BSFC (lb fuel/ hp-hr)	Intake Air Temp (°F)	Exhaust Gas Temp (°F)
3000	4.7	100	40.9	99.79	9.76	10.23	2.09	94	536
4000	5.8	100	38.3	128.47	13.83	9.29	2.38	96	638
6000	13.7	100	59.8	221.36	20.84	10.62	1.52	96	811
Compression Ratio = 8.4									
3000	4.3	100	37.7	102.99	9.91	10.39	2.32	84	425
4000	5.6	100	36.8	130.17	15.58	8.36	2.81	84	489
5000	6.2	100	32.6	164.20	19.08	8.61	3.08	84	557

APPENDIX B
Engineering Drawings

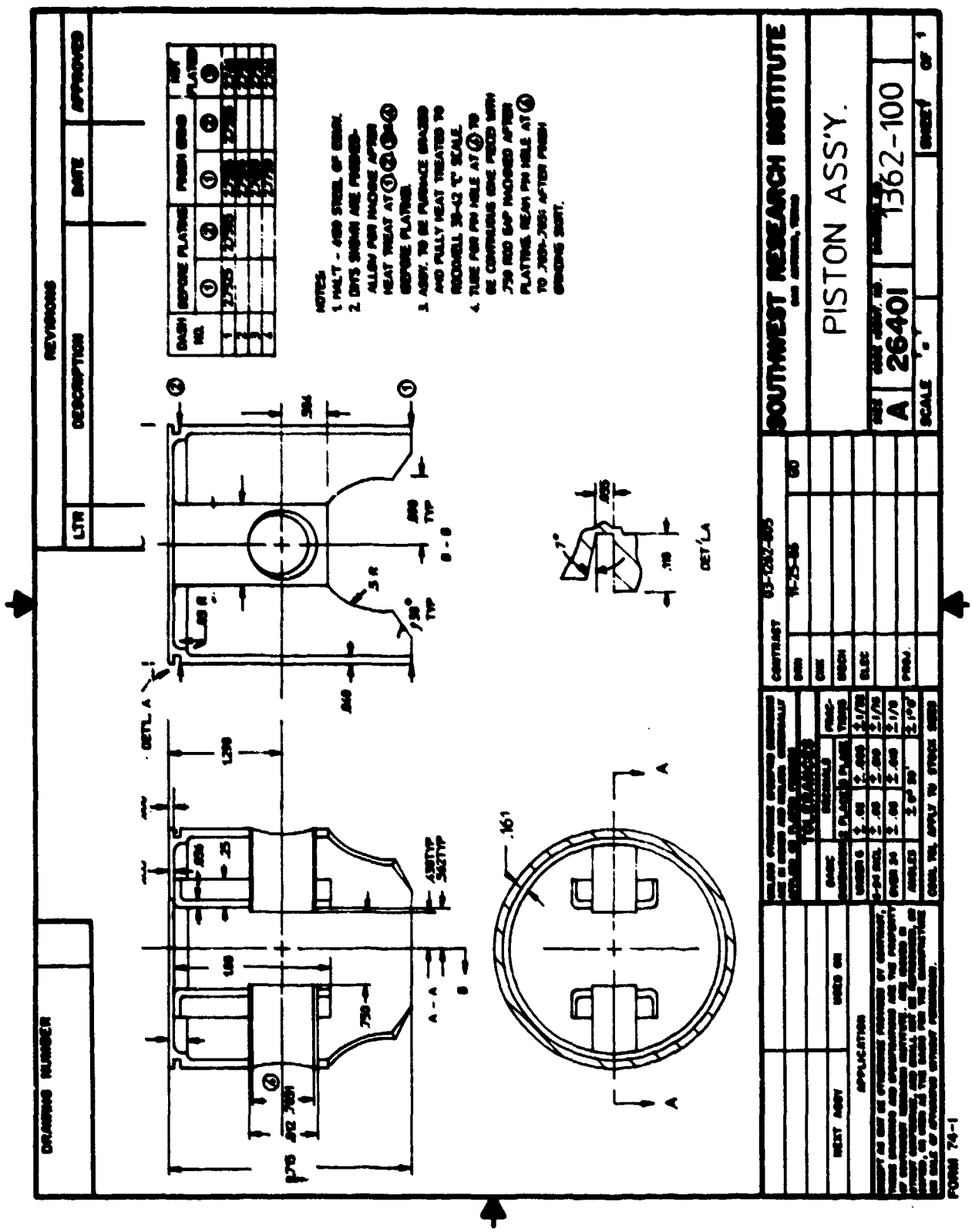

STEEL PISTON ENGINEERING DRAWING

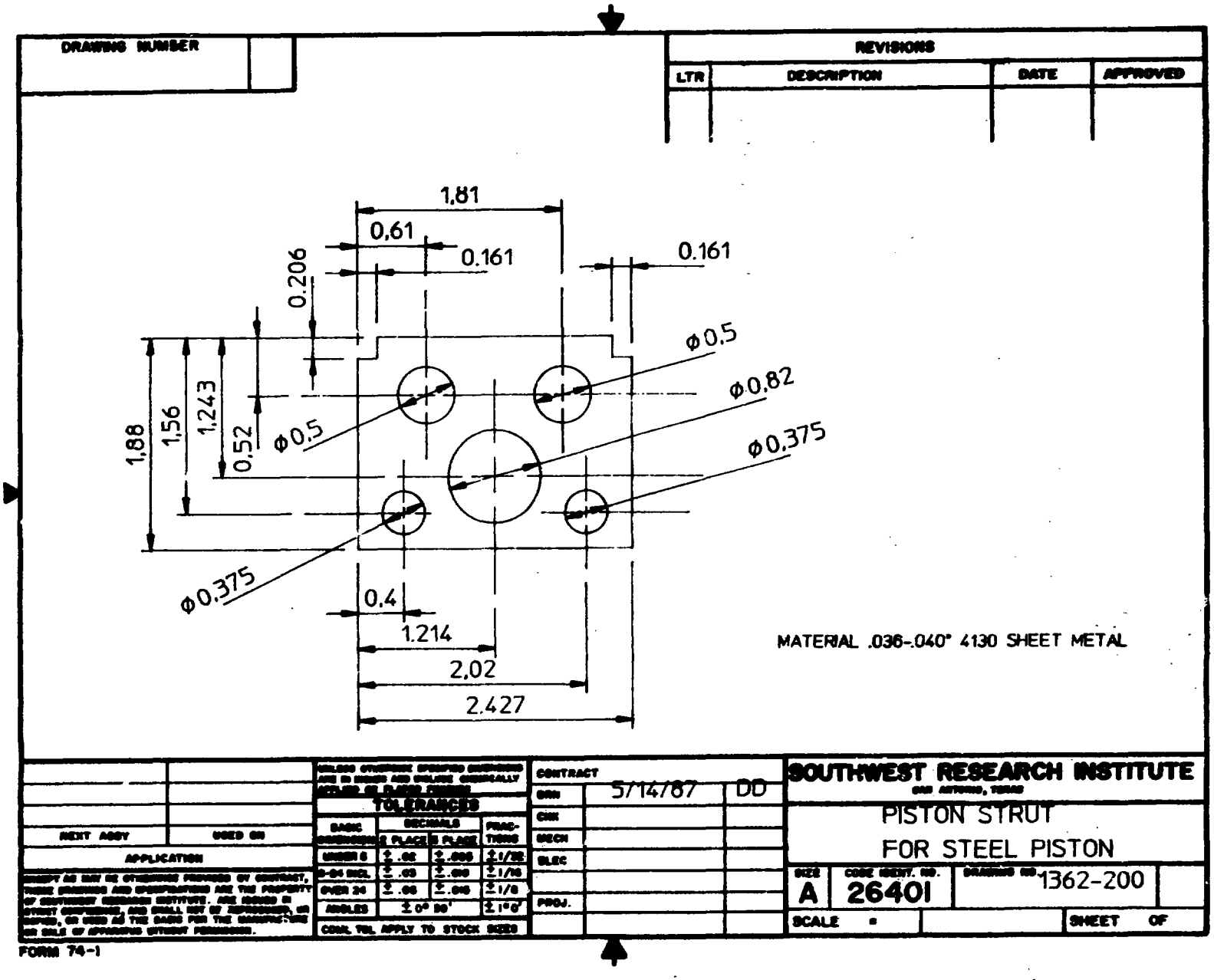

ENGINEERING DRAWING FOR STEEL PISTON SUPPORT STRUTS